Assessment of the SMAP Level-4 Surface and Root-Zone Soil Moisture Product Using *In Situ* Measurements

Rolf H. Reichle[1], Gabrielle J. M. De Lannoy[2], Qing Liu[1,3], Joseph V. Ardizzone[1,3], Andreas Colliander[4], Austin Conaty[1,3], Wade Crow[5], Thomas J. Jackson[5], Lucas A. Jones[6], John S. Kimball[6], Randal D. Koster[1], Sarith P. Mahanama[1,3], Edmond B. Smith[1,3], Aaron Berg[7], Simone Bircher[8], David Bosch[9], Todd G. Caldwell[10], Michael Cosh[5], Ángel González-Zamora[11], Chandra D. Holifield Collins[12], Karsten H. Jensen[13], Stan Livingston[14], Ernesto Lopez-Baeza[15], José Martínez-Fernández[11], Heather McNairn[16], Mahta Moghaddam[17], Anna Pacheco[16], Thierry Pellarin[18], John Prueger[19], Tracy Rowlandson[7], Mark Seyfried[20], Patrick Starks[21], Zhongbo Su[22], Marc Thibeault[23], Rogier van der Velde[22], Jeffrey Walker[24], Xiaoling Wu[24], and Yijian Zeng[22]

Journal of Hydrometeorology

Submitted: 7 Apr 2017
Revised: 10 Jul 2017

[1]NASA Goddard Space Flight Center, Greenbelt, MD, USA
[2]KU Leuven, Heverlee, Belgium
[3]Science Systems and Applications, Inc., Lanham, MD, USA
[4]Jet Propulsion Laboratory, Pasadena, CA, USA
[5]USDA ARS Hydrology and Remote Sensing Laboratory, Beltsville, MD, USA
[6]University of Montana, Missoula, MT, USA
[7]Department of Geography, University of Guelph, Guelph, Ontario, Canada
[8]CESBIO, University of Toulouse, CNES/CNRS/IRD/UPS, Toulouse, France
[9]USDA ARS Southeast Watershed Research, Tifton, GA, USA
[10]Jackson School of Geosciences, University of Texas at Austin, Austin, TX, USA
[11]University of Salamanca, Villamayor, Spain
[12]USDA ARS Southwest Watershed Research Center, Tucson, AZ, USA
[13]Department of Geosciences and Natural Resource Management, University of Copenhagen, Copenhagen, Denmark
[14]USDA ARS National Soil Erosion Research Lab, West Lafayette, IN, USA
[15]University of Valencia, Valencia, Spain
[16]Agriculture and Agri-Food Canada, Ottawa, Ontario, Canada
[17]University of Southern California, Los Angeles, CA, USA
[18]University of Grenoble Alpes, CNRS, IRD, Grenoble INP, IGE, Grenoble, France
[19]USDA ARS National Laboratory for Agriculture and the Environment, Ames, IA, USA
[20]USDA ARS Northwest Watershed Research Center, Boise, ID, USA
[21]USDA ARS Grazinglands Research Laboratory, El Reno, OK, USA
[22]Faculty of Geo-Information Science and Earth Observations (ITC), University of Twente, Enschede, Netherlands
[23]Comisión Nacional de Actividades Espaciales, Buenos Aires, Argentina
[24]Monash University, Clayton, Victoria, Australia

Corresponding author address:
Rolf H. Reichle

NASA Goddard Space Flight Center
Global Modeling and Assimilation Office (Code 610.1)
8800 Greenbelt Road
Greenbelt, MD 20771
USA

Tel.: 301-614-5693
Email: rolf.reichle@nasa.gov

Abstract

The Soil Moisture Active Passive (SMAP) mission Level-4 Surface and Root-Zone Soil Moisture (L4_SM) data product is generated by assimilating SMAP L-band brightness temperature observations into the NASA Catchment land surface model. The L4_SM product is available from 31 March 2015 to present (within 3 days from real-time) and provides 3-hourly, global, 9-km resolution estimates of surface (0-5 cm) and root-zone (0-100 cm) soil moisture and land surface conditions. This study presents an overview of the L4_SM algorithm, validation approach, and product assessment versus *in situ* measurements. Core validation sites provide spatially averaged surface (root-zone) soil moisture measurements for 43 (17) "reference pixels" at 9-km and 36-km grid-cell scales located in 17 (7) distinct watersheds. Sparse networks provide point-scale measurements of surface (root-zone) soil moisture at 406 (311) locations. Core validation site results indicate that the L4_SM product meets its soil moisture accuracy requirement, specified as an unbiased RMSE (ubRMSE, or standard deviation of the error) of 0.04 $m^3 m^{-3}$ or better. The ubRMSE for L4_SM surface (root-zone) soil moisture is 0.038 $m^3 m^{-3}$ (0.030 $m^3 m^{-3}$) at the 9-km scale and 0.035 $m^3 m^{-3}$ (0.026 $m^3 m^{-3}$) at the 36-km scale. The L4_SM estimates improve (significantly at the 5% level for surface soil moisture) over model-only estimates, which do not benefit from the assimilation of SMAP brightness temperature observations and have a 9-km surface (root-zone) ubRMSE of 0.042 $m^3 m^{-3}$ (0.032 $m^3 m^{-3}$). Time series correlations exhibit similar relative performance. The sparse network results corroborate these findings over a greater variety of climate and land cover conditions.

1. Introduction

The Soil Moisture Active Passive (SMAP) mission has been providing global observations of L-band (1.4 GHz) passive microwave brightness temperature since 31 March 2015 at about 40-km resolution from a 685-km, near-polar, sun-synchronous orbit (Entekhabi et al. 2010a; Piepmeier et al. 2017). These observations are highly sensitive to surface soil moisture and temperature, which impact the land surface water and energy balance through, for example, the partitioning of rainfall into runoff and infiltration, and the partitioning of net radiation into latent and sensible heat fluxes. Thus, SMAP observations can be used to enhance our understanding of processes that link the water, energy, and nutrient cycles, and, ultimately, to extend the capabilities of current weather and climate prediction models (Entekhabi et al. 2014).

L-band brightness temperature observations and surface soil moisture retrievals similar to those from SMAP are also available from the Soil Moisture Ocean Salinity (SMOS) mission, launched in November 2009 (Kerr et al. 2010; De Lannoy et al. 2015). Moreover, surface soil moisture retrievals are available from a variety of past and current, active and passive satellite sensors, including the Advanced Microwave Scanning Radiometers (Mladenova et al. 2014; Parinussa et al. 2015) and the Advanced Scatterometer (Wagner et al. 2013). Because the latter instruments take measurements at C- and/or X-band (i.e., at frequencies higher than L-band), they provide observations that have slightly higher spatial resolution but are more sensitive to vegetation and thus less sensitive to soil conditions than SMOS and SMAP, resulting in noisier and less accurate soil moisture retrievals (Kerr et al. 2016). In addition to satellite retrievals, global soil moisture data are also available from reanalysis products (Saha et al. 2010; Dee et al. 2011; Gelaro et al. 2017) and operational numerical weather prediction systems (de Rosnay et al. 2013; Lucchesi

2013a). Some of these model-based products assimilate surface observations to improve the quality of the soil moisture estimates. For example, the SM-DAS-2 product (Albergel et al. 2012) assimilates ASCAT surface soil moisture retrievals and screen-level air temperature and humidity measurements. Furthermore, precipitation observations are used in several reanalysis products, including the Climate Forecasting System Reanalysis (Saha et al. 2010), MERRA-Land (Reichle et al. 2011), ERA-Interim/Land (Balsamo et al. 2015), and MERRA-2 (Reichle et al. 2017a,b).

The SMAP Level-4 Surface and Root-Zone Soil Moisture (L4_SM) product is generated using a land data assimilation system that combines the advantages of space-borne L-band brightness temperature measurements, precipitation observations, and land surface modeling (section 2). The land model's key strength is its reliance on conservation principles for water (converting precipitation inputs into evaporation, runoff, and storage change) and energy (converting incident radiation into outgoing radiation, latent heat flux, sensible heat flux, storage change, and other miscellaneous terms). Given realistic forcing data, these conservation principles ensure at least some first-order reliability in the simulation products, which are then further corrected through the assimilation of SMAP brightness temperature observations.

The L4_SM assimilation system provides two major and invaluable benefits for soil moisture estimation. First, the system facilitates complete coverage in space and time (as opposed to just the times and locations of satellite overpasses). Second, the embedded land model provides a means for producing soil moisture estimates at levels below the ~0-5 cm surface layer that is directly sampled by the satellite instrument. By design, the L4_SM surface and deeper layer soil

moisture estimates are consistent with the available SMAP satellite observations. That is, during the course of the data assimilation process, the subsurface transport formulations in the land model (along with the subsurface assimilation updates) effectively propagate the surface soil moisture and temperature information that is contained in the SMAP brightness temperatures into the deeper soil levels. The L4_SM product thus facilitates the use of SMAP data in applications that require complete spatio-temporal coverage and/or knowledge of deeper-layer soil moisture. The latter is particularly relevant for drought monitoring, water resource management, and sub-seasonal to seasonal climate forecasting.

The SMAP L4_SM product is available every three hours on a global grid with 9-km spacing, thereby interpolating and extrapolating the coarser-scale (~40 km) SMAP observations in time and in space (both horizontally and vertically). The product is published within about 3 days from the time of observation, with the latency primarily dictated by the availability of the gauge-based precipitation product used to drive the land model (Reichle and Liu 2014).

The main objective of this study is to assess the quality of the L4_SM soil moisture and temperature estimates versus *in situ* measurements. In the following, we describe the L4_SM algorithm and product (section 2), discuss our validation approach (section 3), evaluate the L4_SM product against *in situ* measurements (section 4), and provide a summary and conclusions (section 5). A companion paper (Reichle et al. 2017c) assesses the internal diagnostics of the L4_SM algorithm, including the observation-minus-forecast residuals and the analysis increments. Their key findings, updated from (Reichle et al. 2016a), confirm that the

L4_SM analysis is unbiased and produces realistic soil moisture and soil temperature increments that result in spatially consistent soil moisture and temperature analysis fields.

2. L4_SM Algorithm and Data Product

Reichle et al. (2014) and De Lannoy and Reichle (2016a,b) provide a detailed description of the Goddard Earth Observing System, version 5 (GEOS-5), land data assimilation system (LDAS), which forms the basis of the L4_SM algorithm. Here, we briefly summarize their discussion, highlight key features of the L4_SM system, and point out differences between the L4_SM algorithm and the SMOS assimilation described in (De Lannoy and Reichle 2016a,b).

a. Overview

The L4_SM algorithm, shown schematically in Figure 1, is a customized version of the ensemble-based GEOS-5 LDAS built around the GEOS-5 Catchment Land Surface Model (hereinafter "Catchment model"; Koster et al. 2000; Ducharne et al. 2000). The primary drivers of this system are the SMAP L1C_TB brightness temperature observations (section 2d) and the surface meteorological forcing data from the GEOS-5 atmospheric assimilation system, corrected with precipitation observations (section 2b). The SMAP brightness temperature observations are merged with the model estimates using a spatially distributed ensemble Kalman filter (EnKF; section 2d). Briefly, the L4_SM algorithm interpolates and extrapolates the information from the SMAP observations and the model estimates in time and in space, taking into consideration the relative uncertainties of each; the L4_SM data product represents the merged information.

The L4_SM data are generated and distributed on the global, cylindrical, 9-km Equal-Area Scalable Earth, version 2 (EASEv2) grid (Brodzik et al. 2012). The L4_SM outputs include soil moisture estimates for the "surface" (0-5 cm), "root-zone" (0-100 cm) and "profile" (0 cm to

177 depth of bedrock) layers. A single "root-zone" depth was chosen in the modeling system to
178 make the SMAP product more straightforward; in nature, the depths tapped by roots vary with
179 vegetation type, soil type, and other environmental factors (Jackson et al. 1996). Along with soil
180 moisture, a large number of related land surface variables are also available in the L4_SM
181 product, including soil temperature, snow mass, land surface fluxes, surface meteorological
182 forcing data, assimilation diagnostics, and land model parameters. L4_SM surface soil
183 temperature estimates are for the 0-10 cm layer except for tropical (broadleaf evergreen) forests,
184 which are not considered here. The L4_SM soil temperature and snow estimates can be used to
185 screen or flag the L4_SM soil moisture output for times and locations with frozen or snow-
186 covered ground.
187
188 The generation of the L4_SM product involves three basic time scales: (i) the land model
189 computational time step of 7.5 min, (ii) the 3-hour EnKF analysis update time step, and (iii) the
190 3-hour reporting (or output) time step for the published instantaneous and time-average output
191 fields. The available SMAP brightness temperature observations are assimilated in an EnKF
192 analysis update step at the nearest 3-hourly analysis time (0z, 3z, …, and 21z). The latest
193 L4_SM data are generated operationally once per day by the NASA Global Modeling and
194 Assimilation Office and then automatically delivered to the National Snow and Ice Data Center
195 (NSIDC), where they become available to the public almost immediately.
196
197 Here, we use L4_SM Version 2 data (Science Version ID: Vv2030) for the period from April
198 2015 to November 2016. Specifically, we use 3-hourly, instantaneous "analysis" soil moisture
199 and soil temperature fields from the "analysis update" files (Reichle et al. 2016b) and time-

invariant land model parameters (including soil porosity and wilting point) from the "land-model-constants" file (Reichle et al. 2016c). Note that 3-hourly time-average soil moisture and many other land surface fields are provided in the "geophysical" files (Reichle et al. 2016d). See (Reichle et al. 2015a) and the NSIDC website (https://nsidc.org/data/smap/) for complete lists of the available data fields and further details about data product specifications.

b. Modeling system

In the Catchment model, the vertical character of soil moisture for each grid cell is determined (i) by the spatially varying equilibrium profile (defined by a balance of gravity and capillary forces) from the surface to the spatially (horizontally and vertically) varying water table (related to the model's "*catchment deficit*" prognostic variable) and (ii) by two additional model prognostic variables that describe the average deviations from the equilibrium profiles in the 0-100 cm root-zone layer ("*root-zone excess*") and in the 0-5 cm surface layer ("*surface excess*"). The volumetric soil moisture estimates provided in the L4_SM product are diagnosed from these three model prognostic variables.

The Catchment model differs from traditional, layer-based models by including an explicit treatment of the spatial variation of soil water and water table depth within each 9-km grid cell based on the statistics of the catchment topography. This spatial variation enters into the calculation of moisture diffusion between the root-zone and deeper soil moisture storage. The treatment of spatial heterogeneity also allows for the diagnostic separation of each grid cell into "saturated", "unsaturated", and "wilting" sub-grid areas whose sizes vary dynamically. The surface energy balance is computed separately for each sub-grid area using physics specific to its

corresponding hydrological regime. For example, transpiration may be water-limited in the "unsaturated" sub-grid area while it is energy-limited in the "saturated" sub-grid area. This entails the monitoring of independent prognostic surface ("skin") temperature variables for each sub-grid area, which in turn interact with an underlying, six-layer heat diffusion model for soil temperature that is common to all three sub-grid areas. A three-layer snow model component describes the state of the snow pack in terms of snow water equivalent, snow depth, and snow heat content (Stieglitz et al. 2001).

The Catchment model version and parameters of the (Version 2) L4_SM system match those of MERRA-2 (Reichle et al. 2017b; their Table 2) except for the following four differences: (i) the L4_SM soil hydraulic parameters are based on the pedotransfer functions of Wösten et al. (2001) applied to soil textures from the Harmonized World Soil Database (version 1.21) and the State Soil Geographic (STATSGO2) project (labeled "REV" in De Lannoy et al. 2014b); (ii) the WEMIN snow parameter, which governs the model's snow depletion curve, is set to 13 kg m^{-2} (Reichle et al. 2017b); (iii) the leaf area index is based on a merger of data from the Moderate-resolution Imaging Spectroradiometer (MODIS) and the GEOLAND product (Mahanama et al. 2015); and (iv) the surface turbulence scheme is that of Louis (1979). For further details see De Lannoy and Reichle (2016a; their section 2b).

The observation-minus-forecast brightness temperature residuals needed in the soil moisture analysis (section 2d) are computed by converting the Catchment model soil moisture and temperature estimates into estimates of L-band brightness temperatures using a zero-order "tau-omega" radiative transfer model (RTM; De Lannoy et al. 2013). Select RTM input parameters,

including the microwave surface roughness, vegetation structure parameter, and scattering albedo, were calibrated prior to the SMAP launch using multi-angular L-band brightness temperature observations from SMOS (De Lannoy et al. 2014a). This calibration ensured that the long-term mean and variance of the modeled brightness temperatures match those of SMOS. Residual seasonal biases are addressed through rescaling (section 2d).

The Catchment model is driven with surface meteorological forcing data from the GEOS-5 forward-processing (FP) system at 0.25°×0.3125° (latitude × longitude) resolution (GEOS-5.13.0 prior to 1 May 2015, then GEOS-5.13.1 until 24 January 2017, and GEOS-5.16 thereafter; Lucchesi 2013a). The GEOS-5 precipitation data are corrected with gauge-based precipitation observations from the NOAA Climate Prediction Center Unified (CPCU; Xie et al. 2007; Chen et al. 2008) product (Figure 1). The CPCU data are scaled to the climatology of the Global Precipitation Climatology Project, version 2.2 (GPCPv2.2; Adler et al. 2003; Huffman et al. 2009) pentad precipitation product. The precipitation corrections are applied in full within 42.5° latitude from the Equator except in Africa, where no corrections are applied because too few gauges are available there. Between 42.5° and 62.5° latitude (in the Northern and Southern Hemispheres), the precipitation corrections are linearly tapered between full corrections (at 42.5° latitude) and no corrections (at 62.5° latitude). Poleward of 62.5° latitude, the model is forced with the uncorrected GEOS-5 FP precipitation. See Reichle and Liu (2014) and Reichle et al. (2017a) for further details on the precipitation correction algorithm.

c. Nature Run (NRv4) simulation

A longer-term, model-only simulation termed the Nature Run, version 4 (NRv4), was conducted for the period from 2001 through present. NRv4 is a single-member, unperturbed simulation using the Catchment model version of the L4_SM algorithm on the same 9-km EASEv2 grid. Through 2013, the model is driven with surface meteorological forcing from the GEOS-5.9.1 forward-processing for instrument teams (FP-IT) product at 0.5°×0.625° (latitude × longitude) resolution (Lucchesi 2013b). Thereafter, forcing is from the GEOS-5 FP product at 0.25°×0.3125° resolution (GEOS-5.11.0 prior to 1 Aug 2014, as for L4_SM thereafter). The precipitation corrections used for NRv4 are the same as for the L4_SM product.

The NRv4 simulation plays three roles in this study. First, the NRv4 simulation provides initial conditions for the ensemble simulation required to estimate the brightness temperature rescaling parameters, which in turn provides the ensemble initial conditions for the L4_SM simulation starting 31 March 2015 at 0z. (NRv4 was itself spun up for 15 years.) Second, the NRv4 simulation provides the multi-year climatological information needed to (i) calibrate the L4_SM RTM parameters, (ii) determine the parameters that convert L4_SM root-zone and profile soil moisture from volumetric to percentile units, and (iii) calibrate the Level-4 Carbon algorithm (Jones et al. 2017). Third, the NRv4 outputs provide a model-only reference skill against which the impact of the SMAP observations on the skill of the L4_SM product can be measured (section 4).

d. Assimilation of SMAP brightness temperature observations

The Version 2 L4_SM algorithm assimilates horizontally (H) and vertically (V) polarized SMAP brightness temperature observations from the Version 3 SMAP L1C_TB product (Chan et al. 2016a) after averaging the fore- and aft-looking measurements provided in the L1C_TB product on their native 36-km EASEv2 grid. Brightness temperatures from the ascending (~6pm Equator crossing) and descending (~6am Equator crossing) half-orbits are assimilated. The Version 2 L4_SM algorithm does not assimilate data products that are based on the SMAP radar, which failed on 7 July 2015.

The ensemble-based L4_SM data assimilation algorithm is shown schematically in Figure 1 of De Lannoy and Reichle (2016b), but note that for the L4_SM system discussed here the model is on the 9-km grid and the assimilated SMAP observations are only available for a single, 40° incidence angle. The EnKF updates in the L4_SM algorithm are spatially distributed in the sense that all observations within a radius of 1.25° impact the analysis at a given 9-km grid cell (De Lannoy and Reichle 2016b; their section 3.1). The weight of an observation-minus-forecast residual towards the soil moisture (and temperature) increments at a given 9-km grid cell is proportional to the modeled error correlations between the brightness temperature at the observation location and the soil moisture (and temperature) at the location of the increment. This correlation-based weight typically decays with increasing distance of the observation from the location of the increment. The L4_SM system uses 24 ensemble members. The perturbation parameters for the model forcing and prognostic variables match those of De Lannoy and Reichle (2016a; their Table 2) except that the spatial correlation scale for the model prognostics perturbations is set to 0.3° in the L4_SM system.

Seasonally varying bias in the modeled brightness temperatures is addressed prior to assimilation by converting the observations and model forecast brightness temperatures into anomalies from their respective long-term mean seasonal cycles. Since the brightness temperature is strongly impacted by the surface temperature and the RTM parameters, this is done separately for each 36-km grid cell, polarization, and orbit direction (i.e., time-of-day). For details, see De Lannoy and Reichle (2016a; their section 3b and Figures 1 and 2). For the Version 2 L4_SM system, the mean seasonal cycles for the assimilated SMAP brightness temperatures were estimated from SMOS (version 5) observations for the period July 2010 to June 2014, after interpolating the SMOS data to the 40° SMAP incidence angle (De Lannoy et al. 2015). The mean seasonal cycles for the modeled brightness temperatures were computed from sub-sampled model output (at the times and locations of SMOS overpasses), generated with the ensemble L4_SM modeling system using surface meteorological forcing as for NRv4 (section 2c).

Only SMAP brightness temperature observations deemed to be of good quality are assimilated (that is, the lowest bit of the L1C_TB quality flag must equal zero). Moreover, observations that fall outside the natural range between 100 K and 320 K are excluded from the assimilation. Observations are further screened based on the modeled soil temperature (must be greater than 273.35 K) and snow mass (must be less than 10^{-4} kg m^{-2}) to exclude times and locations with frozen or snow-covered soil conditions, for which the RTM is not valid. Finally, the (hourly) precipitation rate at the observation time and location must be less than 2 mm h^{-1} to minimize the detrimental impact of standing water on the analysis. These model-based conditions must be satisfied for all 9-km grid cells within a radius of 40 km from the center point of the observation.

The total brightness temperature observation error standard deviation is set to a constant value of 4 K. This error includes the instrument error (~1.3 K; Piepmeier et al. 2017) and the much larger representativeness error (~3.8 K). The latter consists of all errors associated with the observation operator, including errors in the approximation of the footprint of the satellite observations as well as errors in the RTM-based conversion of the model state vector into brightness temperatures. Since for a given brightness temperature observation only about 50 percent of the signal originates from a circle with a radius of 20 km, we assume an isotropic spatial correlation length for the observation error of 0.25°. Observation errors of H- and V-polarization brightness temperatures are assumed to be uncorrelated, even though this assumption is likely wrong for the representativeness error component. The estimates for the observation and model error parameters used in the L4_SM system are similar to those of De Lannoy and Reichle (2016a,b) and are motivated by the positive results obtained with the assimilation of SMOS observations. Results presented below demonstrate that the assimilation of SMAP data with these error settings also produces skill enhancements. Further refinement of the error parameters may lead to additional skill improvements but is left for future work.

3. Validation Approach and Measurements

The L4_SM product is primarily validated through comparison with independent *in situ* measurements (section 4). Suitable measurements fall into two main categories: (i) For a limited set of climate and land cover conditions, "core validation site" measurements provide accurate estimates of soil moisture at the 9-km or 36-km scales of the model and satellite estimates (section 3b). (ii) For a much wider range of conditions, "sparse network" measurements provide soil moisture estimates at a single, point-scale location within a 9-km model grid cell (section 3c).

a. L4_SM accuracy requirement, validation metrics, and processing of in situ measurements

The accuracy requirement for the L4_SM surface and root-zone soil moisture estimates is that their average unbiased RMSE (ubRMSE) versus *in situ* measurements must be less than 0.04 m^3 m^{-3} (excluding regions of snow and ice, frozen ground, mountainous topography, open water, urban areas, and vegetation with water content greater than 5 kg m^{-2}). The ubRMSE is the RMSE computed after removing the long-term mean bias from the data, also referred to as the standard deviation of the error (Entekhabi et al. 2010b; Reichle et al. 2015b, their Appendix A). The meeting of the requirement is verified by comparing the L4_SM estimates to the 9-km grid-cell scale *in situ* measurements from the core validation sites (section 3b).

In addition to the ubRMSE, we also determine the time series correlation coefficient R and the bias. The latter is computed as the mean of the differences between the L4_SM (or NRv4) estimates and the in situ measurements (that is, estimates minus measurements). Metrics are computed wherever suitable *in situ* measurements are available, including for densely vegetated

or topographically complex areas outside of the limited geographic region for which the 0.04 m^3 m^{-3} validation criterion applies. Metrics are computed using 3-hourly data for the period 1 April 2015 to 31 March 2017 if at least 480 data points are available. All *in situ* measurements used here are subjected to extensive automated and manual quality control procedures following Liu et al. (2011), De Lannoy et al. (2014b), Entekhabi et al. (2014), and Reichle et al. (2015b; their Appendix C) to remove spikes, temporal inhomogeneities, oscillations, and other artifacts commonly seen in automated measurements. Moreover, we exclude times when the soil temperature is below 4°C or when the soil is partially or fully snow covered.

Surface soil moisture and temperature are validated against measurements from the uppermost sensor (typically at ~5 cm depth, see below). Root-zone soil moisture is validated against vertical averages of *in situ* measurements using weights that are proportional to the spacing of the sensor depths within the 0-100 cm layer (see below). In all cases, the deepest sensors used here are weighted most strongly. Vertical averages are only computed if all sensors within a given profile provide measurements that pass quality control.

For each statistic, we also computed 95% confidence intervals that take into account temporal autocorrelation in the time series (De Lannoy and Reichle 2016a; their section 4b). The metrics provided here are conservative skill estimates because they ignore errors in the *in situ* measurements. Triple Collocation techniques could be used to correct for such errors (Chen et al. 2017) but are not considered here. In any case, the *relative* performance of the L4_SM and NRv4 estimates does not depend on the use of Triple Collocation approaches.

b. Core validation site measurements

Core validation sites have locally dense sensor networks that provide accurate soil moisture and soil temperature measurements at the grid-cell scale of the L4_SM product. For any given core validation site, however, the spatial distribution of the *in situ* sensors is typically not aligned with the grid cells of the standard EASEv2 grid. Therefore, we defined custom "shifted" grid cells (or "reference pixels") that better exploit the spatial coverage of the *in situ* measurements at each site, but that do not necessarily align with the standard EASEv2 grid (for examples, see Figure 4 of Colliander et al. 2017). The grid-cell scale measurements are then computed as the weighted average of the contributing sensor measurements using Thiessen polygons or, if available, custom upscaling functions derived from intensive field campaigns (Colliander et al. 2017; their Figure 7).

A core validation site may provide *in situ* measurements for one or more 9-km and/or 36-km reference pixels. Core validation site reference pixels must satisfy a number of criteria, including verification through an intensive field campaign and provision of a minimum number and representative distribution of sensors within the reference pixel (Reichle et al. 2015b, their section 6.2; Colliander et al. 2017). For the comparison against the *in situ* measurements, the 9-km L4_SM estimates are interpolated bi-linearly to the location of the 9-km reference pixels and are aggregated (using area-weighted averaging) for comparison to the 36-km reference pixel estimates. A repeat of the assessment using nearest-neighbor interpolation resulted in skill differences that were much smaller than the typical differences between the L4_SM and NRv4 skill metrics (not shown).

Table 1 lists the core validation sites and reference pixels used here consisting of a total of 43 reference pixels from 19 different core validation sites. Table 2 breaks down the number of core validation sites and reference pixels with suitable quantities of measurements by variable and by horizontal scale. Surface soil moisture measurements are available for all 43 reference pixels. Root-zone soil moisture measurements are available for only 17 reference pixels. Root-zone soil moisture measurements at the 9-km scale are available from only 6 different sites, all of which are in North America (Little Washita, Fort Cobb, Little River, South Fork, Kenaston, and TxSON). Surface soil temperature measurements at 6am (6pm) are available for 35 (36) references pixels. Average metrics across all reference pixels of a given horizontal scale (9-km or 36-km) are computed using the arithmetic average of the metrics at the individual reference pixels. The 95% confidence intervals are first averaged in the same way and then divided by the square root of the number of different core validation sites contributing to the metric (as listed in Table 2).

Table 1 also lists the depths of the shallowest sensors, which are used to validate the L4_SM surface soil moisture and surface soil temperature estimates. Moreover, Table 1 provides the depths of the deepest sensors that contribute to the *in situ* root-zone soil moisture measurements. At all reference pixels except Little River and Yanco, the deepest sensors are at 45 cm or 50 cm depth. At Little River, the deepest sensors are at 30 cm depth. At Yanco, the deepest sensors are installed vertically and centered at depths of 45 cm and 75 cm, representing the 30-60 cm and 60-90 cm layers, respectively. For many sites, individual sensors tend to drop out temporarily, which leads to undesirable discontinuities in the reference pixel average soil moisture. To mitigate this effect, we require at least 8 individual, complete sensor profiles (after quality

control) to compute the reference pixel average, provided at least 8 sensor profiles were in the ground. For the 17 reference pixels that are based on fewer than 8 sensor profiles, we require data from all contributing sensor profiles (after quality control) to compute the reference pixel average. The time-average number of individual sensors that contribute to any given 36-km reference pixel average ranges between 6 and 33.2 for surface soil moisture (Table 1), with a mean value of 15.3 (not shown). At the 9-km scale, 14 of the 26 surface reference pixels are based on fewer than 8 individual sensor profiles, while the rest of the 9-km reference pixels have 8 or more sensor profiles each (Table 1), with a mean value of 7.4 across all 9-km reference pixels (not shown).

c. Sparse network measurements

The defining feature of sparse network measurements is that there is usually just one sensor (or profile of sensors) located within a given 9-km EASEv2 grid cell. The sparse network measurements used here include data from the USDA Natural Resources Conservation Service Soil Climate Analysis Network (SCAN; Schaefer et al. 2007), the US Climate Reference Network (USCRN; Bell et al. 2013; Diamond et al. 2013), the Oklahoma Mesonet (McPherson et al. 2007), and the OzNet in Australia's Murrumbidgee catchment (Smith et al. 2012). Note that for the Australian data, the core validation site and the sparse network results are not independent because about three quarters of the OzNet sites also contributed to the grid-cell scale soil moisture measurements of the Yanco reference pixels.

Table 3 lists the number of sparse network sites with sufficient data after quality control. Across all networks, 406 locations have surface and 311 have root-zone soil moisture measurements.

475 Most of the sites are in the continental United States, including about 100 each in the USCRN
476 and SCAN networks, and another 100 in Oklahoma from the Mesonet. OzNet contributes 42
477 sites with surface soil moisture measurements, 18 of which also provide root-zone
478 measurements. Moreover, Table 3 lists the measurement depths used for computing root-zone
479 measurements. For SCAN and USCRN sites, measurements at 50 cm (and occasionally 100 cm)
480 depth are available. It is, however, very difficult to take and verify such deeper layer
481 measurements consistently over long periods of time. These measurements are therefore not of
482 the quantity and quality required for L4_SM validation and are not used here. For OzNet, the
483 measurements at the 45 cm depth are used as root-zone measurements.
484
485 The sparse network measurements are compared to the L4_SM and NRv4 data from the standard
486 9-km EASEv2 grid cell that includes the sensor location. Spatially averaged skill metrics are
487 calculated by clustering sites geographically to keep densely sampled areas from dominating the
488 validation metrics and to ensure realistic confidence intervals (De Lannoy and Reichle 2016a).
489 The number of clusters is estimated a priori after prescribing an average cluster radius of 1.5°,
490 which is similar to the 1.25° compact support length scale of the L4_SM analysis (section 2d).
491 The 95% confidence intervals are first averaged in the same way and then divided by the square
492 root of the number of clusters.
493
494 Sparse network results are grouped into locations with "favorable" or "unfavorable" conditions
495 for soil moisture estimation from space-borne brightness temperature observations. Favorable
496 locations include all areas where the accuracy requirement (section 3a) applies. Unfavorable
497 locations include areas where (i) the maximum climatological leaf area index exceeds 5 m^2 m^{-2}

(MODIS 2008), (ii) the predominant land cover is forest, wetland, or urban according to the International Geosphere-Biosphere Programme (IGBP) DISCover (Loveland et al. 2000) vegetation classification, (iii) the topography is complex (elevation standard deviation greater than 71 m), or (iv) the elevation of the sensor location differs by more than 500 m from the mean elevation of the surrounding 36-km grid cell. The above grouping is determined using the land cover, vegetation, and topography parameters of the L4_SM modeling system (Mahanama et al. 2015).

4. Results

In this section, we present a detailed, quantitative analysis of the skill of the L4_SM soil moisture and temperature estimates in reproducing *in situ* measurements from the core validation sites (section 4a) and sparse networks (section 4b). Some of the text in this section is from two non-peer reviewed project reports (Reichle et al. 2015b, 2016a) and has been updated to reflect the results obtained for the Version 2 L4_SM product and the longer validation period used here.

a. Core site validation

In this subsection, we present the validation results using core site measurements. We first discuss the soil moisture validation results for three representative reference pixels (Little Washita, Little River, and South Fork) that exemplify features of the L4_SM estimates and indicate aspects needing improvement. For reference, Table 4 lists the metrics for all 43 reference pixels. Thereafter, we present average soil moisture and temperature metrics across all reference pixels and demonstrate that the L4_SM product meets its accuracy requirement.

1) LITTLE WASHITA (OKLAHOMA)

The Little Washita, Oklahoma, site is situated in grasslands in a temperate, sub-humid climate. Based on several field campaigns that addressed *in situ* sensor calibration and upscaling (Cosh et al. 2006), the confidence in the quality of the *in situ* estimates at this site is very high, and good product performance at this site is considered to be important. Figure 2 shows the L4_SM, NRv4, and *in situ* time series for the 36-km reference pixel. (The results for the 9-km reference pixel at Little Washita are qualitatively similar, but there are long gaps in the *in situ* measurements.) Soil moisture varies considerably during the validation period, owing to the

exceptionally wet conditions during May 2015 and the very dry conditions in August and September of both years. The L4_SM and NRv4 estimates clearly capture the overall variability, as well as the timing of the major rainstorms. However, neither the NRv4 nor the L4_SM estimates fully capture the wet conditions starting in late October 2015 and lasting through the winter of 2015-2016. Nevertheless, the time series correlation coefficients are very high, with R values of 0.81 for L4_SM surface soil moisture and 0.88 for L4_SM root-zone soil moisture, which is an improvement over the already high values of 0.73 and 0.87 for NRv4 surface and root-zone soil moisture, respectively (Table 4).

The improvement is also reflected in the ubRMSE metric, which decreases from 0.037 $m^3 m^{-3}$ for NRv4 surface soil moisture to 0.033 $m^3 m^{-3}$ for L4_SM, and from 0.029 $m^3 m^{-3}$ for NRv4 root-zone soil moisture to 0.024 $m^3 m^{-3}$ for L4_SM (Table 4). The improvements are mostly due to the increased dynamic range and the generally faster dry-downs of the L4_SM estimates resulting from the assimilation of the SMAP observations, which leads to a better match of the dry-downs indicated by the *in situ* measurements. Bias values are very low for surface soil moisture (around -0.01 $m^3 m^{-3}$ for L4_SM and NRv4). Root-zone soil moisture, however, is generally too dry and somewhat more biased for L4_SM (-0.043 $m^3 m^{-3}$) than for NRv4 (-0.037 $m^3 m^{-3}$).

2) LITTLE RIVER (GEORGIA)

The Little River, Georgia, site is in a humid agricultural environment, includes a substantial amount of tree cover, and has sandy soils. The site is also subject to irrigation and located near ephemeral, forested wetlands that can flood following rain events, but neither irrigation nor

553 wetland processes are considered in the L4_SM modeling system. As for the Little Washita site,
554 we show time series for the 36-km reference pixel at Little River (Figure 3) because of gaps in
555 the *in situ* measurements at the 9-km reference pixel. All time series reflect a drop from
556 somewhat wetter conditions in April and May of both years to drier summer conditions, with
557 frequent yet typically modest rain events (Figure 3). The frequent wetting and drying events
558 shown in the *in situ* measurements are reasonably captured by the L4_SM and NRv4 estimates,
559 but the exact timing and magnitude of the storms and dry-downs is less certain. Moreover, the
560 tree cover, sandy soils, and irrigation at Little River complicate the modeling of soil moisture
561 and brightness temperature, resulting in overall slightly lower skill values than for Little
562 Washita.
563
564 Despite the above complications, NRv4 estimates have reasonable skill, and the assimilation of
565 SMAP observations again results in skill improvement. Surface soil moisture has an R value of
566 0.68 for NRv4, which improves to 0.76 for L4_SM. The correlation for root-zone soil moisture
567 is higher, with R values of 0.81 for NRv4 and 0.84 for L4_SM (Table 4). The assimilation also
568 improves the ubRMSE values for surface soil moisture estimates from 0.044 $m^3 m^{-3}$ for NRv4 to
569 0.035 $m^3 m^{-3}$ for L4_SM and for root-zone soil moisture estimates from 0.033 $m^3 m^{-3}$ for NRv4
570 to 0.025 $m^3 m^{-3}$ for L4_SM. Bias values are relatively high at ~0.10 $m^3 m^{-3}$ for surface soil
571 moisture and ~0.07 $m^3 m^{-3}$ for root-zone soil moisture. The SMAP and SMOS passive soil
572 moisture retrievals also exhibit a wet bias (Chan et al. 2016b), which may be related to the
573 ephemeral wetlands in the vicinity of the site. The wet bias in the NRv4 estimates, however,
574 suggests that errors in the Catchment model parameters are the main reason for the wet bias in
575 L4_SM.

Figure 3 also reveals residual minor issues with the *in situ* measurements. Between May 17 and June 5, 2015, for example, the reference pixel average root-zone soil moisture shows somewhat erratic behavior. In this particular case, bad data from one sensor passed the automated quality control, and sensors also dropped out repeatedly during the period in question. The impact of these residual issues are very minor and do not impact our main conclusions.

3) SOUTH FORK (IOWA)

South Fork, Iowa, is in a cold climate agricultural region dominated by summer crops of corn and soybeans. Conditions in winter are mostly bare soil or stubble, followed by intensive tillage in early April that creates large surface roughness, which subsequently decreases again with additional soil treatments and rainfall, and as crops begin to cover the surface. Such variations in surface roughness are difficult to capture in the (climatological) microwave RTM parameters of the L4_SM algorithm and in soil moisture retrieval algorithms in general (Patton and Hornbuckle 2013). Moreover, at the 9-km and 36-km scales considered here, the land cover is a mix of corn and soybeans, which usually rotate each year, although there has been a trend toward more corn in recent years. By early July, for example, corn typically has a high vegetation water content of ~3 kg m^{-2} while that of soybeans is typically much smaller (around 0.3 kg m^{-2}) (Jackson et al. 2004). Finally, owing to the high clay content of the soils in this region, the agricultural fields are equipped with tiles to improve drainage. This local feature is not captured in the global-scale Catchment model of the L4_SM algorithm.

598 Figure 4 shows soil moisture time series for a 9-km reference pixel at South Fork. Soil moisture
599 conditions during the warm season are dominated by approximately weekly rain events with
600 subsequent dry-downs. The L4_SM surface soil moisture estimates capture this pattern and
601 present a clear improvement over NRv4, especially in 2016. This is reflected in the ubRMSE
602 values, which decrease from 0.070 $m^3 m^{-3}$ for NRv4 to 0.053 $m^3 m^{-3}$ for L4_SM (Table 4). The
603 surface soil moisture R value increases considerably from 0.08 for NRv4 to 0.62 for L4_SM.
604 Root-zone metrics show similar improvements for L4_SM over NRv4, with ubRMSE values
605 decreasing from 0.044 $m^3 m^{-3}$ for NRv4 to 0.031 $m^3 m^{-3}$ for L4_SM and R values increasing
606 considerably from 0.03 for NRv4 to 0.58 for L4_SM. Generally, however, the L4_SM estimates,
607 and even more so the NRv4 estimates, do not capture the larger dynamic range of the *in situ*
608 observations, which may be a reflection of the tile drainage. Bias values range from 0.075 m^3
609 m^{-3} for NRv4 surface soil moisture to -0.014 $m^3 m^{-3}$ for L4_SM root-zone soil moisture.
610
611 4) SOIL MOISTURE SUMMARY METRICS
612 We now discuss the average soil moisture metrics across all reference pixels (section 3b), shown
613 separately for the 9-km and 36-km reference pixels in Figure 5 (with numerical values listed in
614 the bottom two rows of Table 4). The most important result is that the average ubRMSE values
615 for L4_SM surface soil moisture (0.038 $m^3 m^{-3}$) and root-zone soil moisture (0.030 $m^3 m^{-3}$) at the
616 9-km scale meet the accuracy requirement of 0.04 $m^3 m^{-3}$.
617
618 For a more in-depth analysis, we first compare the skill of the L4_SM and NRv4 estimates. For
619 the ubRMSE and R metrics and at the 9-km and the 36-km scales, the surface soil moisture skill
620 of L4_SM exceeds that of NRv4 by a statistically significant margin (as indicated by the non-

621 overlapping confidence intervals; Figure 5). For example, the 9-km ubRMSE for L4_SM
622 surface soil moisture is 0.038 $m^3 m^{-3}$, compared to 0.042 $m^3 m^{-3}$ for NRv4. The corresponding R
623 values are 0.67 for L4_SM and 0.58 for NRv4. The average bias is slightly (but not
624 significantly) worse for L4_SM (0.046 $m^3 m^{-3}$) than NRv4 (0.043 $m^3 m^{-3}$). The results are
625 similar for root-zone soil moisture, except here the differences between the L4_SM and NRv4
626 estimates are not significant (Figure 5). The 9-km ubRMSE for L4_SM root-zone soil moisture
627 (0.030 $m^3 m^{-3}$) is slightly lower than that of NRv4 (0.032 $m^3 m^{-3}$), and the R value for L4_SM
628 (0.70) is higher than that of NRv4 (0.56). The average root-zone soil moisture bias is
629 remarkably small and slightly better for L4_SM (0.009 $m^3 m^{-3}$) than NRv4 (0.019 $m^3 m^{-3}$).
630
631 A closer look at the metrics for the individual reference pixels (Table 4) reveals that the
632 ubRMSE and R metrics are worse for L4_SM than NRv4 at some sites, including Carman and
633 HOBE. There could be several reasons why the L4_SM analysis degrades the model-only skill,
634 including site-specific errors in the radiative transfer modeling. For example, the L4_SM system
635 does not account for the heavy dewfall and the variety of different crops at Carman. At HOBE,
636 the SMOS-based brightness temperature climatology used for rescaling might be impacted by
637 radio-frequency interference or by the effect of the land-sea contrast in the interferometric
638 processing (Al Bitar et al. 2012). Nevertheless, the L4_SM product has, on balance, higher skill
639 than NRv4. The L4_SM root-zone ubRMSE is below the 0.04 $m^3 m^{-3}$ threshold at all 16 (9-km
640 and 36-km) reference pixels, while the NRv4 ubRMSE exceeds 0.04 $m^3 m^{-3}$ at 2 of the 3 South
641 Fork reference pixels. Surface soil moisture estimates from NRv4 fail to meet the 0.04 $m^3 m^{-3}$
642 threshold at 18 of the 43 reference pixels. By contrast, L4_SM surface soil moisture estimates
643 fail to meet the threshold at only 10 of the 43 reference pixels, including 9-km pixels at Yanco,

644 Carman, St. Josephs, South Fork, Benin, and TxSON. This result further illustrates the key role
645 played by the assimilation of SMAP observations in meeting the L4_SM accuracy requirement
646 (which applies to the average ubRMSE across all 9-km reference pixels; section 3a).
647
648 Next, we compare the skill values at 9-km reference pixels to those at the 36-km scale.
649 Generally, the L4_SM and NRv4 skill at 36 km is better for all three metrics than that at 9 km
650 (Figure 5), which is consistent with the fact that the model forcing data and the assimilated
651 SMAP brightness temperature observations are all at resolutions of about 30 km or greater. The
652 information used to downscale the assimilated information stems only from the land model
653 parameters, which are at the finer, 9-km resolution. It is therefore not surprising that the L4_SM
654 (and NRv4) estimates are more skillful (that is, contain less random error) when averaged to the
655 36-km scale than at the 9-km scale. Perhaps the biggest difference between the 36-km and 9-km
656 reference pixel skill is for the surface soil moisture bias (Figure 5b). The smaller bias at the
657 36-km scale is likely also related to the fact that the grid-cell scale *in situ* measurements for
658 36-km reference pixels are typically based on more individual sensor locations than those for
659 9-km reference pixels, resulting in more robust *in situ* estimates of the true long-term mean
660 conditions at the 36-km scale.
661
662 Finally, we compare the skill of the surface soil moisture estimates to that of the root-zone
663 estimates. Across all scales and metrics and for the L4_SM and NRv4 estimates, the skill of the
664 root-zone soil moisture estimates is always better than that of the surface estimates (Figure 5).
665 This result makes sense because there is much more variability in surface soil moisture.
666
667

5) SOIL TEMPERATURE SUMMARY METRICS

Since the focus of the L4_SM product is on soil moisture, there is no pre-defined accuracy target for the L4_SM surface soil temperature estimates. It is nevertheless instructive to assess their skill (Figure 6; Table 5), especially given the importance of soil temperature for biophysical processes and the use of L4_SM soil temperature estimates as inputs to the SMAP Level-4 Carbon product (Jones et al. 2017). The average surface soil temperature metrics for L4_SM and NRv4 are fairly similar across all categories, with average ubRMSE values ranging from 1.6 to 1.8 K (Figure 6a) and average R values of ~0.97 (Figure 6c) for 9-km and 36-km estimates at 6am and 6pm. At 6am, surface soil temperature estimates from L4_SM have a slightly lower ubRMSE than NRv4 (by ~0.1 K) and a slightly higher R value than NRv4 (by ~0.005), but the differences are not significant. At 6pm, the L4_SM and NRv4 ubRMSE and R values are essentially identical.

Somewhat bigger differences between the various estimates occur for the average bias in surface soil temperature (Figure 6b). At 6am, both L4_SM and NRv4 are biased cold, with NRv4 having a larger (negative) bias of around -2.5 K compared to about -1.8 K for L4_SM (at both the 9-km and 36-km scales). This 6am cold bias is consistent with a known nighttime cold bias in the GEOS-5 modeling system (Chan et al. 2016b). At 6pm, the average bias at the 9-km scale nearly vanishes for NRv4 (0.1 K), whereas L4_SM still exhibits a distinct cold bias (-1.1 K). Note that some of the bias at individual sites might also be caused by instrumentation details such as the vertical or horizontal installation of the sensors, which impacts the exact depths where the sensors' thermistors are located.

691 The 36-km average bias shown in Figure 6b includes the extreme values at the Ngari reference
692 pixel in western Tibet, where the 6pm bias in surface soil temperature is -9.1 K for NRv4 and
693 -12.5 K for L4_SM (Table 5). The L4_SM bias at Ngari is not unique for a global modeling
694 system. In their Table 3, Su et al. (2013) report a diurnal mean bias of -6.9 K at Naqu (in central
695 Tibet) for surface soil temperature estimates from the operational system of the European Centre
696 for Medium-Range Weather Forecasts. The reasons for the extreme bias in Tibet are complex.
697 Most importantly, there is a bias in the GEOS-5 radiation and air temperature forcing data used
698 in the L4_SM system compared to the observation-based data of Chen et al. (2011) (not shown).
699 This forcing bias is likely compounded by errors in the L4_SM soil texture inputs, soil thermal
700 parameters, and surface turbulence parameterization (Van der Velde et al. 2009; Zeng et al.
701 2012; Zheng et al. 2015). If Ngari is excluded from the 36-km reference pixel average, the 6pm
702 bias values change from -0.5 K to 0.2 K for NRv4 and from -1.7 K to -0.9 K for L4_SM. More
703 generally, the increase in the (absolute) bias in the L4_SM estimates compared to NRv4 is likely
704 the result of using imperfect brightness temperature rescaling parameters (section 2d), but this
705 requires further investigation and is left for future study.
706
707 The relatively minor differences between the L4_SM and NRv4 soil temperature metrics (Figure
708 6) are not surprising. The L4_SM brightness temperature analysis has been calibrated primarily
709 for updating the model forecast soil moisture estimates; soil temperature increments are
710 relatively small by design (De Lannoy and Reichle 2016a). This strategy mirrors the approach
711 taken by the SMAP and SMOS (passive) soil moisture retrieval algorithms, which rely on
712 ancillary soil temperature information that is assumed to be sufficiently accurate to invert
713 brightness temperature observations into soil moisture estimates.

714

715 *b. Sparse network validation*

716 Figure 7 illustrates the ubRMSE values for the L4_SM estimates at the sparse network sites. The
717 gray background shading in the figure also indicates whether a site is within the mask of the
718 formal accuracy requirement (section 3a). The resulting delineation (Figure 7) suggests, for
719 example, that sites in the more topographically complex western United States mountain areas
720 and in the more densely vegetated portions of the eastern United States fall, as expected, outside
721 the mask. Overall, ubRMSE values range from 0.02 $m^3 m^{-3}$ to 0.07 $m^3 m^{-3}$, with generally lower
722 error values for root-zone soil moisture than for surface soil moisture (Figure 7). Errors are
723 generally lowest in dry and mountainous areas in the western United States, where the soil
724 moisture variability is typically low, thus naturally limiting the ubRMSE values. The ubRMSE
725 values at the Australian sites are relatively high both inside and outside the mask (on average,
726 0.063 $m^3 m^{-3}$ for surface and 0.056 $m^3 m^{-3}$ for root-zone soil moisture), owing primarily to the
727 large variability in soil moisture in this region. The R values for the sparse network sites, shown
728 in Figure 8, range from 0.3 to 0.9, with generally similar correlations for surface and root-zone
729 soil moisture. There is no obvious spatial pattern across the US networks or the Australian sites,
730 although the latter exhibit generally high R values.

731

732 Figure 9 shows the average L4_SM metrics vs. sparse network measurements, broken down by
733 the exclusion mask of the accuracy requirement (as indicated by the gray shading in Figures 7
734 and 8). The figure confirms that the L4_SM ubRMSE values are lower at the sites outside the
735 mask, with values of 0.049 $m^3 m^{-3}$ for surface soil moisture and 0.040 $m^3 m^{-3}$ for root-zone soil
736 moisture (Figure 9b, Table 6), compared to 0.054 $m^3 m^{-3}$ and 0.044 $m^3 m^{-3}$ for surface and root-

737 zone soil moisture, respectively, at sites within the mask (Figure 9a). Again, this result is related
738 to the much lower variability of soil moisture in the arid regions of the western United States,
739 which also happen to lie largely in mountainous terrain. The result is reversed for the average
740 bias. Inside the mask, average bias values are 0.028 $m^3 m^{-3}$ for surface soil moisture and -0.003
741 $m^3 m^{-3}$ for root-zone soil moisture (Figure 9c), compared to 0.078 $m^3 m^{-3}$ for surface soil
742 moisture and 0.042 $m^3 m^{-3}$ for root-zone soil moisture, respectively, outside the mask (Figure
743 9d). This relative performance is at least partly due to the increased topographical complexity
744 near many of the sites outside of the mask, which are generally even less representative of the
745 grid-cell average conditions than are sparse network sites within the mask. The values for the
746 time series correlation coefficients generally range between 0.6 and 0.7 and are more similar
747 inside and outside the mask (Figure 9e,f). This is expected because the R values are, by
748 construction, insensitive to bias and to errors in variability.
749
750 Figure 9 also shows the skill of the NRv4 estimates. The surface soil moisture skill in terms of R
751 is significantly higher (at the 5% level) for L4_SM than for NRv4, reflecting the additional
752 information contributed by the assimilation of the SMAP brightness temperature observations in
753 the L4_SM system both inside and outside of the exclusion mask. For root-zone soil moisture,
754 the skill values are very similar for L4_SM and NRv4. As for the core validation sites, the
755 typically small differences between L4_SM and NRv4 estimates reflect the fact that the sparse
756 network measurements are located in areas where the surface meteorological forcing takes
757 advantage of high-quality, gauge-based precipitation measurements. Larger improvements from
758 the assimilation of SMAP observations can be expected in areas where the precipitation forcing

759 inputs are not as well informed by gauge measurements, as demonstrated by Bolten and Crow
760 (2012) for the assimilation of AMSR-E soil moisture retrievals.
761
762 Table 6 further provides average skill metrics broken down by the IGBP land cover classes
763 (section 3c). The ubRMSE and R skill of the L4_SM surface and root-zone soil moisture
764 estimates is better than that of NRv4 for all IGBP classes except for root-zone soil moisture in
765 grasslands and urban areas, where NRv4 is better than L4_SM (but not significantly). The bias
766 values listed in Table 6 suggest that the mean soil moisture from the L4_SM estimates is biased
767 high (that is, wet) for all land cover classes, with similar mean bias values for NRv4. This is
768 particularly true for the forest class, because *in situ* measurement sites are typically on grassy
769 areas, regardless of the surrounding land cover. For the forest class, Table 6 shows that the
770 L4_SM and NRv4 estimates have the highest bias values, ~0.1 $m^3 m^{-3}$ for surface soil moisture
771 and 0.055 $m^3 m^{-3}$ for root-zone soil moisture (not considering the higher average root-zone bias
772 at the three sites in the urban class).
773
774
775
776
777
778

5. Summary and Conclusions

This study provides a brief overview of the SMAP L4_SM algorithm and focuses on the validation of the L4_SM product using *in situ* soil moisture and temperature measurements from core validation sites and sparse networks. Based on the core validation site results, the L4_SM estimates of surface and root-zone soil moisture meet the accuracy requirement (ubRMSE ≤ 0.04 $m^3 m^{-3}$). For surface soil moisture, the ubRMSE is 0.038 $m^3 m^{-3}$ at the 9-km scale and 0.035 m^3 m^{-3} at the 36-km scale. For root-zone soil moisture, the ubRMSE is 0.030 $m^3 m^{-3}$ at the 9-km scale and 0.026 m^3 m^{-3} at the 36-km scale (Figure 5). Through the assimilation of SMAP brightness temperatures, the L4_SM surface soil moisture estimates are improved significantly (at the 5% level) compared to model-only NRv4 estimates. The latter have an ubRMSE of 0.042 $m^3 m^{-3}$ at the 9-km scale and do not meet the L4_SM accuracy requirement. L4_SM root-zone soil moisture estimates are also better (but not significantly) than those of NRv4, which have an ubRMSE of 0.032 $m^3 m^{-3}$ at the 9-km scale. Similar qualitative results are obtained for the R metric.

Surface soil temperature ubRMSE values vs. core validation site measurements range between 1.6 and 1.8 K for 6am and 6pm estimates from L4_SM and NRv4 at the 9-km and 36-km scales (Figure 6). The L4_SM estimates show only minor improvements (not significant) of ~0.1 K for 6am (compared to NRv4), with nearly identical 6pm skill values for L4_SM and NRv4. R values for surface soil temperature estimates are ~0.97, suggesting that the modeled soil temperatures adequately capture synoptic and seasonal variations. The L4_SM product is biased cold by about -2 K at 6am, which is consistent with a known cold bias in current GEOS-5 products. In the arid, high-elevation environment at Ngari in western Tibet, however, errors in

802 the L4_SM forcing data and modeling system result in a much larger cold bias of -12.5 K for
803 surface soil temperature at 6pm.
804
805 The sparse network results corroborate the core validation site findings for a greater variety of
806 climate and land cover conditions (Figure 9). It is important to keep in mind that the sparse
807 network skill metrics presented here underestimate the true skill because these metrics are based
808 on a direct comparison of the L4_SM product against *in situ* measurements which are subject to
809 upscaling and other errors. The same is true, to a lesser extent, for the metrics vs. core validation
810 site measurements, and Chen et al. (2017) quantified the impact of such errors on the R skill of
811 soil moisture retrievals. Therefore, the sparse network ubRMSE values suggest that the L4_SM
812 estimates would meet the formal accuracy requirement across a very wide variety of surface
813 conditions, beyond those that are covered by the few core validation sites that have been
814 available to date for formal verification of the accuracy requirement. The sparse network results
815 thus provide additional confidence in the conclusions drawn from the core validation site
816 comparisons.
817
818 The core validation site and sparse network results both suggest that the L4_SM surface soil
819 moisture is still biased wet (by 0.02-0.05 m^3 m^{-3}, on average), while the root-zone soil moisture
820 bias is smaller (less than 0.01 m^3 m^{-3} for the core sites, and 0.016 m^3 m^{-3} for the sparse network
821 sites). The wet bias in surface soil moisture is consistent with the findings of De Lannoy et al.
822 (2014b), who introduced the revised soil texture and soil hydraulic parameters used here to
823 address the even stronger bias in earlier versions of the GEOS-5 modeling system (such as those
824 used in the MERRA-Land and MERRA-2 reanalysis products). The development of the L4_SM

825 product played an important role in mitigating the bias of GEOS-5 soil moisture estimates, and
826 work is ongoing to further reduce the remaining bias.
827
828 The skill of the model-only NRv4 estimates (section 2c) rests, to a large degree, on the accuracy
829 of the precipitation forcing, which relies on the daily, 0.5°, gauge-based CPCU product (except
830 in Africa and the high latitudes). For the most part, the soil moisture validation against *in situ*
831 measurements is limited to regions that also have relatively accurate precipitation inputs, which
832 implies that the model-only (NRv4) skill is already relatively high, thereby limiting the potential
833 improvements that can be obtained from the assimilation of SMAP observations. In regions with
834 poor precipitation data, the impact of the SMAP observations should be larger, but the precise
835 benefit remains unknown in those regions because they also lack soil moisture *in situ*
836 measurements suitable for validation. In future work, we plan to quantify the skill improvement
837 against model-only estimates that do not benefit from the use of gauge-based precipitation data.
838
839 The NRv4 and L4_SM estimates differ in that the NRv4 estimates are from a single-member
840 model run without perturbations, whereas the L4_SM estimates are based on an ensemble of
841 model realizations that experiences perturbations to its model forcing and prognostic variables.
842 An undesirable, yet at this time unavoidable, side effect of the perturbations regime is that it
843 leads to biases between the ensemble mean estimates and the estimates from the unperturbed
844 NRv4 model integration. This is particularly acute in very arid regions, where the perturbations
845 in soil moisture are, by construction, biased wet because the unperturbed, single-member model
846 run often remains at the lowest possible soil moisture value, thereby making negative (that is,
847 drying) perturbations unphysical. Some of the differences between the NRv4 and L4_SM

848 estimates will therefore partly reflect the impact of the perturbations regime rather than the use
849 of SMAP observations. We plan to investigate this issue further by generating a model-only
850 ensemble run with the same perturbations regime as the L4_SM product but without SMAP
851 assimilation. Preliminary results based on a small domain suggest that the relative performance
852 of the L4_SM estimates and the revised model-only estimates is quite similar to that of L4_SM
853 and NRv4.
854
855 Our assessment of the Version 2 L4_SM data is still quite limited by the period of record. The
856 two years of data that were available for this study do not yet cover a representative range of
857 inter-annual variability. As the SMAP observatory and *in situ* networks continue to provide
858 additional measurements, the reliability of future assessments will increase. Moreover,
859 enhancements in the GEOS-5 modeling system and in the L-band brightness temperature
860 climatology needed for bias correction are expected to improve the quality of the L4_SM
861 product. In particular, the L-band brightness temperature climatology will eventually be based
862 on SMAP (as opposed to SMOS) observations. This will improve the brightness temperature
863 bias correction and permit the use of SMAP data in regions where SMOS observations are
864 contaminated by radio-frequency interference.
865
866 Finally, the validation of the L4_SM product against *in situ* measurements must be viewed in
867 conjunction with other assessments. For example, Crow et al. (2017) demonstrated for the
868 south-central US that L4_SM soil moisture estimates have significantly improved utility for
869 forecasting the streamflow response to future rainfall events (relative to that of soil moisture
870 retrievals from L-band and higher-frequency Tb observations). Moreover, Reichle et al. (2016a,

871 2017c) evaluate the statistics of the observation-minus-forecast (O-F) residuals and the analysis
872 increments from the L4_SM algorithm, which are available wherever and whenever SMAP
873 observations are assimilated, thereby providing a more global perspective of the algorithm's
874 performance.
875
876
877

Acknowledgments

Funding for this work was provided by the NASA SMAP mission. Computational resources were provided by the NASA High-End Computing program through the NASA Center for Climate Simulation. We are grateful for the datasets and data archiving centers that supported this work and appreciate those who make the generation, dissemination, and validation of the L4_SM product possible, including SMAP team members at JPL, GSFC, and NSIDC and staff at NOAA CPC, NOAA NCEI, USDA ARS, USDA NRCS, the Oklahoma Climatological Survey, and Monash University. Erica Tetlock is acknowledged for her help with the Kenaston network, for which funding was provided by the Canadian Space Agency and by Environment and Climate Change Canada. We thank three anonymous reviewers for their helpful comments.

889 **References**

890 Adler, R. F., and Coauthors, 2003: The version 2 Global Precipitation Climatology Project
891 (GPCP) monthly precipitation analysis (1979–present). *J. Hydrometeor.*, **4**, 1147–1167,
892 doi:10.1175/1525-7541(2003)004<1147:TVGPCP>2.0.CO;2.

893 Al Bitar, A., and Coauthors, 2012: Evaluation of SMOS Soil Moisture Products Over
894 Continental U.S. Using the SCAN/SNOTEL Network. *IEEE Transactions on Geoscience*
895 *and Remote Sensing*, **50**, 1572-1586, doi:10.1109/TGRS.2012.2186581.

896 Albergel, C., and Coauthors, 2012: Evaluation of remotely sensed and modelled soil moisture
897 products using global ground-based *in situ* observations. *Remote Sensing of Environment*,
898 **118**, 215-226, doi:10.1016/j.rse.2011.11.017.

899 Balsamo, G., and Coauthors, 2015: ERA-Interim/Land: A global land surface reanalysis data set,
900 *Hydrol. Earth Syst. Sci*., **19**, 389-407, doi:10.5194/hess-19-389-2015.

901 Bell, J., and Coauthors, 2013: U.S. Climate Reference Network soil moisture and temperature
902 observations. *J. Hydrometeor*., **14**, 977–988, doi:10.1175/JHM-D-12-0146.1.

903 Bolten, J.D. and W. T. Crow, 2012: Improved prediction of quasi-global vegetation conditions
904 using remotely-sensed surface soil moisture. *Geophysical Research Letters*, **39**, L19406,
905 doi:10.1029/2012GL053470.

906 Brodzik, M. J., B. Billingsley, T. Haran, B. Raup, and M. H. Savoie, 2012: EASE-Grid 2.0:
907 Incremental but Significant Improvements for Earth-Gridded Data Sets. *ISPRS International*
908 *Journal of Geo-Information*, **1**, 32-45, doi:10.3390/ijgi1010032.

909 Chan, S., E. G. Njoku, and A. Colliander, 2016a: SMAP L1C Radiometer Half-Orbit 36 km
910 EASE-Grid Brightness Temperatures, Version 3. Boulder, Colorado USA. NASA National

911 Snow and Ice Data Center Distributed Active Archive Center.
912 doi:10.5067/E51BSP6V3KP7. Last accessed 10 December 2016.
913 Chan, S. K., and Coauthors, 2016b: Assessment of the SMAP Passive Soil Moisture Product.
914 *IEEE Transactions on Geoscience and Remote Sensing*, **54**, 4994-5007,
915 doi:10.1109/TGRS.2016.2561938.
916 Chen, F., and Coauthors, 2017: Application of Triple Collocation in Ground-based Validation of
917 Soil Moisture Active/Passive (SMAP) Level 2 Data Products. *IEEE Journal of Selected*
918 *Topics in Applied Earth Observations and Remote Sensing*, **10**, 489-502,
919 doi:10.1109/JSTARS.2016.2569998.
920 Chen, M., W. Shi, P. Xie, V. B. S. Silva, V. E. Kousky, R. W. Higgins, and J. E. Janowiak, 2008:
921 Assessing objective techniques for gauge-based analyses of global daily precipitation. *J.*
922 *Geophys. Res.*, **113**, D04110, doi:10.1029/2007JD009132.
923 Chen, Y., K. Yang, J. He, J. Qin, J. Shi, J. Du, and Q. He, 2011: Improving land surface
924 temperature modeling for dry land of China. *J. Geophys. Res.*, **116**, D20104,
925 doi:10.1029/2011JD015921.
926 Colliander, A., and Coauthors, 2017: Validation of SMAP surface soil moisture products with
927 core validation sites. *Remote Sensing of Environment,* **191**, 215-231,
928 doi:10.1016/j.rse.2017.01.021.
929 Cosh, M. H., T. J. Jackson, P. J. Starks, and G. Heathman, 2006: Temporal stability of surface
930 soil moisture in the LittleWashita RiverWatershed and its applications in satellite soil
931 moisture product validation. *J. Hydrol.*, **323**, 168–177, doi:10.1016/j.jhydrol.2005.08.020.
932 Crow, W. T., F. Chen, R. H. Reichle, and Q. Liu, 2017: L band microwave remote sensing and
933 land data assimilation improve the representation of prestorm soil moisture conditions for

hydrologic forecasting. *Geophys. Res. Lett.*, **44**, doi:10.1002/2017GL073642.

De Lannoy, G. J. M, R. H. Reichle, and V. R. N. Pauwels, 2013: Global Calibration of the GEOS-5 L-band Microwave Radiative Transfer Model over Nonfrozen Land Using SMOS Observations. *Journal of Hydrometeorology*, **14**, 765-785, doi:10.1175/JHM-D-12-092.1.

De Lannoy, G. J. M., R. H. Reichle, and J. A. Vrugt, 2014a: Uncertainty Quantification of GEOS-5 L-Band Radiative Transfer Model Parameters using Bayesian Inference and SMOS Observations. *Remote Sensing of Environment*, **148**, 146-157, doi:10.1016/j.rse.2014.03.030.

De Lannoy, G. J. M., R. D. Koster, R. H. Reichle, S. P. P. Mahanama, and Q. Liu, 2014b: An Updated Treatment of Soil Texture and Associated Hydraulic Properties in a Global Land Modeling System. *Journal of Advances in Modeling Earth Systems*, **6**, 957-979, doi:10.1002/2014MS000330.

De Lannoy, G. J. M., R. H. Reichle, J. Peng, Y. Kerr, R. Castro, E. Kim, and Q. Liu, 2015: Converting between SMOS and SMAP level-1 brightness temperature observations over nonfrozen land. *IEEE Geosci. Remote Sens. Lett.*, **12**, 1908–1912, doi:10.1109/LGRS.2015.2437612.

De Lannoy, G. J. M., and R. H. Reichle, 2016a: Global Assimilation of Multiangle and Multipolarization SMOS Brightness Temperature Observations into the GEOS-5 Catchment Land Surface Model for Soil Moisture Estimation. *Journal of Hydrometeorology*, **17**, 669-691, doi:10.1175/JHM-D-15-0037.1.

De Lannoy, G. J. M., and R. H. Reichle, 2016b: Assimilation of SMOS Brightness Temperatures or Soil Moisture Retrievals into a Land Surface Model. *Hydrology and Earth System Sciences*, **20**, 4895-4911, doi:10.5194/hess-20-4895-2016.

de Rosnay P., M. Drusch, D. Vasiljevic, G. Balsamo, C. Albergel and L. Isaksen, 2013: A

957 simplified Extended Kalman Filter for the global operational soil moisture analysis at
958 ECMWF. *Q. J. R. Meteorol. Soc.*, **139**, 1199-1213, doi:10.1002/qj.2023.

959 Dee, D., and Coauthors, 2011: The ERA-Interim reanalysis: Configuration and performance of
960 the data assimilation system. Quart. J. Roy. Meteor. Soc., **137**, 553–597, doi:10.1002/qj.828.

961 Diamond, H., and Coauthors, 2013: U.S. Climate Reference Network after one decade of
962 operations: Status and assessment. *Bull. Amer. Meteor. Soc*., **94**, 485–498,
963 doi:10.1175/BAMS-D-12-00170.1.

964 Ducharne, A., R. D. Koster, M. J. Suarez, M. Stieglitz, and P. Kumar, 2000: A catchment-based
965 approach to modeling land surface processes in a general circulation model: 2. Parameter
966 estimation and model demonstration. *J. Geophys. Res.*, **105**(D20), 24,823-24,838,
967 doi:10.1029/2000JD900328.

968 Entekhabi, D., and Coauthors, 2010a: The Soil Moisture Active and Passive (SMAP) Mission.
969 *Proceedings of the IEEE*, **98**, 704-716, doi:10.1109/JPROC.2010.2043918.

970 Entekhabi, D., R. H. Reichle, R. D. Koster, and W. T. Crow, 2010b: Performance Metrics for
971 Soil Moisture Retrievals and Application Requirements. *Journal of Hydrometeorology*, **11**,
972 832-840, doi:10.1175/2010JHM1223.1.

973 Entekhabi, D., and Coauthors, 2014: SMAP Handbook, JPL Publication, JPL 400-1567, NASA
974 Jet Propulsion Laboratory, Pasadena, California, USA, 182 pp. Available online at
975 https://smap.jpl.nasa.gov/mission/description.

976 Gelaro, R., and Coauthors, 2017: MERRA-2 Overview. *J. Climate*, **30**, 5419-5454,
977 doi:10.1175/JCLI-D-16-0758.1.

978 Huffman, G. J., R. F. Adler, D. T. Bolvin, and G. Gu, 2009: Improving the global precipitation
979 record: GPCP version 2.1. Geophys. Res. Lett., **36**, L17808, doi:10.1029/2009GL040000.

Jackson, R. B., J. Canadell, J. R. Ehleringer, H. A. Mooney, O. E. Sala, and E. D. Schulze, 1996: A global analysis of root distributions for terrestrial biomes. *Oecologia*, **108**, 389-411, doi:10.1007/BF00333714.

Jackson, T., D. Chen, M. Cosh, F. Li, M. Anderson, C. Walthall, P. Doraiswamy, and E. R. Hunt, 2004: Vegetation water content mapping using Landsat data derived normalized difference water index (NDWI) for corn and soybean. *Remote Sensing of Environment*, **92**, 475-482.

Jones, L. A., and Coauthors, 2017: The SMAP Level 4 Carbon Product for Monitoring Ecosystem Land-Atmosphere CO2 Exchange. *IEEE Transactions on Geosciences and Remote Sensing*, accepted for publication.

Kerr, Y. H., and Coauthors, 2010: The SMOS mission: New tool for monitoring key elements of the global water cycle. *Proc. IEEE*, **98**, 666–687, doi:10.1109/JPROC.2010.2043032.

Kerr, Y. H., and Coauthors, 2016: Overview of SMOS performance in terms of global soil moisture monitoring after six years in operation. *Remote Sensing of Environment*, **180**, 40-63, doi:10.1016/j.rse.2016.02.042.

Koster, R. D., M. J. Suarez, A. Ducharne, M. Stieglitz, and P. Kumar, 2000: A catchment-based approach to modeling land surface processes in a general circulation model: 1. Model structure. *J. Geophys. Res.*, **105** (D20), 24,809-24,822, doi:10.1029/2000JD900327.

Liu, Q., R. H. Reichle, R. Bindlish, M. H. Cosh, W. T. Crow, R. de Jeu, G. J. M. De Lannoy, G. J. Huffman, and T. J. Jackson, 2011: The contributions of precipitation and soil moisture observations to the skill of soil moisture estimates in a land data assimilation system. *Journal of Hydrometeorology*, **12**, 750-765, doi:10.1175/JHM-D-10-05000.1.

1002 Louis, J. E, 1979: A Parametric Model of Vertical Eddy Fluxes in the Atmosphere. *Bound. Lay.*
1003 *Meteorol.*, **17**, 187-202.
1004 Loveland, T. R., B. C., Reed, J. F. Brown, D. O. Ohlen, Z. Zhu, L. Yang, and J. W. Merchant,
1005 2000: Development of a global land cover characteristics database and IGBP DISCover from
1006 1 km AVHRR data. *International Journal of Remote Sensing*, 21, 1303-1330, doi:
1007 10.1080/014311600210191.
1008 Lucchesi, R. 2013a: File Specification for GEOS-5 FP, NASA GMAO Office Note, No. 4
1009 (Version 1.0), National Aeronautics and Space Administration, Goddard Space Flight
1010 Center, Greenbelt, Maryland, USA, 63pp. Available online at
1011 http://gmao.gsfc.nasa.gov/pubs.
1012 Lucchesi, R. 2013b: File Specification for GEOS-5 FP-IT, NASA GMAO Office Note, No. 2
1013 (Version 1.2), National Aeronautics and Space Administration, Goddard Space Flight
1014 Center, Greenbelt, Maryland, USA, 60pp. Available online at
1015 http://gmao.gsfc.nasa.gov/pubs.
1016 Mahanama, S. P., R. D. Koster, G. K. Walker, L. L. Takacs, R. H. Reichle, G. De Lannoy, Q.
1017 Liu, B. Zhao, and M. J. Suarez, 2015: Land Boundary Conditions for the Goddard Earth
1018 Observing System Model Version 5 (GEOS-5) Climate Modeling System - Recent Updates
1019 and Data File Descriptions. *NASA/TM–2015-104606*, Vol. **39**, National Aeronautics and
1020 Space Administration, Goddard Space Flight Center, Greenbelt, Maryland, USA, 55 pp.
1021 Available from http://gmao.gsfc.nasa.gov/pubs.
1022 McPherson, R. A., and Coauthors, 2007: Statewide Monitoring of the Mesoscale Environment:
1023 A Technical Update on the Oklahoma Mesonet. *J. Atmos. Oceanic Technol.*, **24**, 301–321,
1024 doi: 10.1175/JTECH1976.1.

Mladenova, I.E., and Coauthors, 2014: Remote monitoring of soil moisture using passive microwave-based techniques — theoretical basis and overview of selected algorithms for AMSR-E. *Remote Sens. Environ.*, **144**, 197-213, doi: 10.1016/j.rse.2014.01.013.

MODIS, 2008: Leaf Area Index - Fraction of Photosynthetically Active Radiation 8-Day L4 Global 1km (MOD15A2 v005). NASA EOSDIS Land Processes DAAC, USGS Earth Resources Observation and Science (EROS) Center, Sioux Falls, South Dakota (https://lpdaac.usgs.gov), accessed 28 July 2015, at https://e4ftl01.cr.usgs.gov/MOLT/MOD15A2.005.

Parinussa, R. M., T. R. H. Holmes, N. Wanders, W. A. Dorigo, and R. A. M. de Jeu, 2015: A Preliminary Study toward Consistent Soil Moisture from AMSR2. *J. Hydrometeor.*, **16**, 932–947, doi: 10.1175/JHM-D-13-0200.1.

Patton, J., and B. Hornbuckle, 2013: Initial Validation of SMOS Vegetation Optical Thickness in Iowa, *IEEE Geoscience and Remote Sensing Letters*, **10**, 647-651, doi:10.1109/LGRS.2012.2216498.

Piepmeier, J. R., and Coauthors, 2017: SMAP L-Band Microwave Radiometer: Instrument Design and First Year on Orbit. *IEEE Transactions on Geoscience and Remote Sensing*, **55**, 1954-1966, doi:10.1109/TGRS.2016.2631978.

Reichle, R. H., and Q. Liu, 2014: Observation-Corrected Precipitation Estimates in GEOS-5. *NASA Technical Report Series on Global Modeling and Data Assimilation, NASA/TM-2014-104606,* Vol. **35**, National Aeronautics and Space Administration, Goddard Space Flight Center, Greenbelt, Maryland, USA, 18pp. Available online at http://gmao.gsfc.nasa.gov/pubs.

1047 Reichle, R. H., R. D. Koster, G. J. M. De Lannoy, B. A. Forman, Q. Liu, S. P. P. Mahanama, and
1048 A. Touré, 2011: Assessment and enhancement of MERRA land surface hydrology estimates.
1049 *J. Climate*, **24**, 6322–6338, doi:10.1175/JCLI-D-10-05033.1.

1050 Reichle, R. H., R. Koster, G. De Lannoy, W. Crow, and J. Kimball, 2014: SMAP Level 4
1051 Surface and Root Zone Soil Moisture Data Product: L4_SM Algorithm Theoretical Basis
1052 Document (Revision A). Soil Moisture Active Passive (SMAP) Mission Science Document.
1053 JPL D-66483, Jet Propulsion Laboratory, Pasadena, CA. Available online at
1054 https://nsidc.org/sites/nsidc.org/files/files/data/smap/272_L4_SM_RevA_web.pdf

1055 Reichle, R. H., R. A. Lucchesi, J. V. Ardizzone, G.-K. Kim, E. B. Smith, and B. H. Weiss,
1056 2015a: Soil Moisture Active Passive (SMAP) Mission Level 4 Surface and Root Zone Soil
1057 Moisture (L4_SM) Product Specification Document, *NASA GMAO Office Note, No. 10*
1058 *(Version 1.4)*, National Aeronautics and Space Administration, Goddard Space Flight
1059 Center, Greenbelt, Maryland, USA, 82pp. Available online at
1060 http://gmao.gsfc.nasa.gov/pubs.

1061 Reichle, R. H., and Coauthors, 2015b: Soil Moisture Active Passive (SMAP) Project Assessment
1062 Report for the Beta-Release L4_SM Data Product. *NASA Technical Report Series on Global*
1063 *Modeling and Data Assimilation, NASA/TM-2015-104606, Vol. 40*, National Aeronautics
1064 and Space Administration, Goddard Space Flight Center, Greenbelt, Maryland, USA, 63pp.
1065 Available online at http://gmao.gsfc.nasa.gov/pubs.

1066 Reichle, R. H., and Coauthors, 2016a: Soil Moisture Active Passive Mission L4_SM Data
1067 Product Assessment (Version 2 Validated Release), NASA GMAO Office Note, No. 12
1068 (Version 1.0), National Aeronautics and Space Administration, Goddard Space Flight
1069 Center, Greenbelt, Maryland, USA, 55pp. Available online at

http://gmao.gsfc.nasa.gov/pubs.

Reichle, R. H., G. De Lannoy, R. D. Koster, W. T. Crow, and J. S. Kimball, 2016b*:* SMAP L4 9 km EASE-Grid Surface and Root Zone Soil Moisture Analysis Update, Version 2. Boulder, Colorado USA. NASA National Snow and Ice Data Center Distributed Active Archive Center. doi:10.5067/JJY2V0GJNFRZ. Last accessed 10 December 2016.

Reichle, R. H., G. De Lannoy, R. D. Koster, W. T. Crow, and J. S. Kimball, 2016c*:* SMAP L4 9 km EASE-Grid Surface and Root Zone Soil Moisture Land Model Constants, Version 2. Boulder, Colorado USA. NASA National Snow and Ice Data Center Distributed Active Archive Center. doi:10.5067/VBRUC1AFRQ22. Last accessed 10 December 2016.

Reichle, R. H., G. De Lannoy, R. D. Koster, W. T. Crow, and J. S. Kimball, 2016d*:* SMAP L4 9 km EASE-Grid Surface and Root Zone Soil Moisture Geophysical Data, Version 2. Boulder, Colorado USA. NASA National Snow and Ice Data Center Distributed Active Archive Center. doi:10.5067/YK70EPDHNF0L. Last accessed 10 December 2016.

Reichle, R. H., Q. Liu, R. D. Koster, C. S. Draper, S. P. P. Mahanama, and G. S. Partyka, 2017a: Land surface precipitation in MERRA-2, *Journal of Climate,* **30**, 1643-1664, doi:10.1175/JCLI-D-16-0570.1.

Reichle, R. H., and Coauthors, 2017b: Assessment of MERRA-2 land surface hydrology estimates. *Journal of Climate*, **30**, 2937–2960, doi:10.1175/JCLI-D-16-0720.1.

Reichle, R. H., and Coauthors, 2017c: Global Assessment of the SMAP Level 4 Surface and Root-Zone Soil Moisture Product Using Assimilation Diagnostics. *Journal of Hydrometeorology*, submitted.

Saha, S., and Coauthors, 2010: The NCEP Climate Forecast System Reanalysis. *Bull. Amer.*

Meteor. Soc., **91**, 1015–1057, doi:10.1175/2010BAMS3001.1.

Schaefer, G. L., M. H. Cosh, and T. J. Jackson, 2007: The USDA Natural Resources Conservation Service Soil Climate Analysis Network (SCAN). *J. Atmos. Oceanic Technol*., **24**, 2073– 2077.

Smith, A., and Coauthors, 2012: The Murrumbidgee soil moisture monitoring network data set. *Water Resour. Res.*, **48**, W07701, doi:10.1029/2012WR011976.

Su, Z., P. de Rosnay, J. Wen, L. Wang, and Y. Zeng, 2013: Evaluation of ECMWF's soil moisture analyses using observations on the Tibetan Plateau. *J. Geophys. Res. Atmos.*, **118**, 5304–5318, doi:10.1002/jgrd.50468.

Stieglitz, M., A. Ducharne, R. Koster, and M. Suarez, 2001: The Impact of Detailed Snow Physics on the Simulation of Snow Cover and Subsurface Thermodynamics at Continental Scales. *J. Hydrometeor.*, **2**, 228-242.

Van der Velde, R., Z. Su, M. Ek, M. Rodell, and Y. Ma, 2009: Influence of thermodynamic soil and vegetation parameterizations on the simulation of soil temperature states and surface fluxes by the noah LSM over a tibetan plateau site. *Hydrology and Earth System Sciences*, **13**, 759.

Wagner, W., and Coauthors, 2013: The ASCAT Soil Moisture Product: A Review of its Specifications, Validation Results, and Emerging Applications. *Meteorologische Zeitschrift*, 22, 5-33, doi:10.1127/0941-2948/2013/0399.

Wösten, J., Y. A. Pachepsky, and W. Rawls, 2001: Pedotransfer functions: Bridging the gap between available basic soil data and missing soil hydraulic characteristics. *J. Hydrol.*, **251**, 123-150, doi:10.1016/S0022-1694(01)00464-4.

Xie, P., M. Chen, S.Yang, A.Yatagai, T.Hayasaka, Y. Fukushima, and C. Liu, 2007: A gauge-based analysis of daily precipitation over East Asia. *J. Hydrometeor.*, **8**, 607–626, doi:10.1175/JHM583.1

Zeng, X., Z. Wang, and A. Wang, 2012: Surface Skin Temperature and the Interplay between Sensible and Ground Heat Fluxes over Arid Regions. *J. Hydrometeor.*, **13**, 1359–1370, doi:10.1175/JHM-D-11-0117.1.

Zheng, D., and Coauthors, 2015: Augmentations to the Noah Model Physics for Application to the Yellow River Source Area. Part II: Turbulent Heat Fluxes and Soil Heat Transport. *J. Hydrometeor.*, **16**, 2677–2694, doi:10.1175/JHM-D-14-0199.1.

Tables

Site Name	Country	Climate Regime	Land Cover	Reference Pixel											
				ID	Latitude [degree]	Longitude [degree]	Horizontal Scale [km]	Depth of Deepest Sensor [m]	Number of Sensors (Surface Soil Moisture)			Number of Sensors (Root Zone Profiles)		
									Min	Mean	Max	Min	Mean	Max
REMEDHUS	Spain	Temperate	Croplands	**03013602**	**41.28**	**-5.41**	**36**	**0.05**	**8**	**14.6**	**17**	n/a	n/a	n/a
				03010903	41.42	-5.37	9	0.05	4	4.0	4	n/a	n/a	n/a
				03010908	41.32	-5.27	9	0.05	4	4.0	4	n/a	n/a	n/a
Reynolds Creek	USA	Arid	Grasslands	**04013603**	**43.14**	**-116.76**	**36**	**0.05**	**8**	**9.5**	**11**	n/a	n/a	n/a
				04010907	43.19	-116.72	9	0.05	4	4.0	4	n/a	n/a	n/a
				04010910	43.09	-116.81	9	0.05	4	4.0	4	n/a	n/a	n/a
Yanco	Australia (New South Wales)	Arid	Cropland / natural mosaic	**07013601**	**-34.85**	**146.17**	**36**	**0.75**	**9**	**25.4**	**28**	**7**	**7.0**	**7**
				07010902	-34.72	146.13	9	0.05	8	10.2	11	n/a	n/a	n/a
				07010916	-34.98	146.31	9	0.05	8	10.3	11	n/a	n/a	n/a
Carman	Canada (Manitoba)	Cold	Croplands	**09013610**	**49.61**	**-97.94**	**36**	**0.05**	**8**	**17.9**	**20**	n/a	n/a	n/a
				09010906	49.67	-97.98	9	0.05	8	10.1	11	n/a	n/a	n/a
Ngari	China (Tibet)	Cold	Barren / sparse	**12033601**	**32.41**	**79.98**	**36**	**0.05**	**6**	**6.0**	**6**	**n/a**	**n/a**	**n/a**
Walnut Gulch	USA (Arizona)	Arid	Shrub open	**16013603**	**31.68**	**-110.04**	**36**	**0.05**	**8**	**10.6**	**12**	n/a	n/a	n/a
				16010906	31.72	-110.09	9	0.05	8	9.6	11	n/a	n/a	n/a
				16010907	31.72	-109.99	9	0.05	8	10.4	11	n/a	n/a	n/a
				16010913	31.83	-110.90	9	0.05	7	7.0	7	n/a	n/a	n/a
Little Washita	USA (Oklahoma)	Temperate	Grasslands	**16023602**	**34.88**	**-98.09**	**36**	**0.45**	**8**	**15.5**	**18**	**8**	**13.4**	**17**
				16020907	34.92	-98.04	9	0.45	4	4.0	4	4	4.0	4
Fort Cobb	USA (Oklahoma)	Temperate	Grasslands	**16033602**	**35.42**	**-98.62**	**36**	**0.45**	**8**	**12.3**	**13**	**8**	**11.1**	**13**
				16030911	35.38	-98.57	9	0.45	4	4.0	4	4	4.0	4
				16030916	35.29	-98.48	9	0.45	4	4.0	4	4	4.0	4
Little River	USA (Georgia)	Temperate	Cropland / natural mosaic	**16043602**	**31.60**	**-83.59**	**36**	**0.30**	**8**	**19.8**	**23**	**8**	**18.6**	**22**
				16040901	31.72	-83.73	9	0.30	8	8.0	8	6	6.0	6
St Josephs	USA (Indiana)	Temperate	Croplands	16060907	41.45	-84.97	9	0.05	8	8.2	9	n/a	n/a	n/a
South Fork	USA (Iowa)	Cold	Croplands	**16073602**	**42.47**	**-93.39**	**36**	**0.50**	**8**	**14.4**	**15**	**8**	**13.1**	**15**
				16070909	42.42	-93.53	9	0.50	4	4.0	4	4	4.0	4
				16070911	42.42	-93.35	9	0.50	4	4.0	4	4	4.0	4
Monte Buey	Argentina	Temperate	Croplands	**19023601**	**-32.96**	**-62.52**	**36**	**0.05**	**8**	**10.3**	**13**	n/a	n/a	n/a
				19020902	-33.01	-62.49	9	0.05	5	5.0	5	n/a	n/a	n/a
Tonzi Ranch	USA	Temperate	Savannas woody	**25013601**	**38.47**	**-121.00**	**36**	**0.05**	**8**	**17.5**	**26**	n/a	n/a	n/a
				25010911	38.43	-120.95	9	0.05	8	17.5	26	n/a	n/a	n/a
Kenaston	Canada (Saskatchewan)	Cold	Croplands	**27013601**	**51.45**	**-106.46**	**36**	**0.50**	**8**	**25.7**	**28**	**8**	**23.1**	**28**
				27010910	51.39	-106.51	9	0.05	8	8.0	8	n/a	n/a	n/a
				27010911	51.39	-106.42	9	0.50	8	13.6	14	8	12.2	14
Valencia	Spain	Cold	Savannas woody	41010906	39.57	-1.26	9	0.05	6	6.0	6	n/a	n/a	n/a
Niger	Niger	Arid	Grassland	**45013601**	**13.59**	**3.65**	**36**	**0.05**	**6**	**6.0**	**6**	n/a	n/a	n/a
				45010902	13.55	2.69	9	0.05	4	4.0	4	n/a	n/a	n/a
Benin	Benin	Tropical	Savannas	**45023601**	**9.77**	**1.68**	**36**	**0.05**	**7**	**7.0**	**7**	n/a	n/a	n/a
				45020902	9.80	1.73	9	0.05	5	5.0	5	n/a	n/a	n/a
TxSON	USA (Texas)	Temperate	Grasslands	**48013601**	**30.31**	**-98.78**	**36**	**0.50**	**10**	**33.2**	**35**	**10**	**26.3**	**28**
				48010902	30.43	-98.82	9	0.50	8	9.9	11	8	8.6	10
				48010911	30.27	-98.73	9	0.50	8	14.4	15	8	13.7	14
HOBE	Denmark	Temperate	Croplands	**67013601**	**55.97**	**9.10**	**36**	**0.05**	**8**	**15.1**	**21**	n/a	n/a	n/a

TABLE 1. Core validation sites and reference pixels. Information for 36-km reference pixels is shown in bold.

	Surface soil moisture		Root zone soil moisture		Surface Soil Temperature (6am)		Surface Soil Temperature (6pm)	
Horizontal scale	36 km	9 km	36 km	9 km	36 km	9 km	36 km	9 km
Number of different core sites	17	17	7	6	14	12	14	13
Number of reference pixels	17	26	7	9	14	21	14	22

1131

1132 TABLE 2. Number of different core sites and number of reference pixels used in the soil moisture

1133 and temperature validation.

1134

1135

Network	Area	Sensor Depths (cm)	N	
			Surface Soil Moisture	Root Zone Soil Moisture
SCAN	USA	5, 10, 20	135	129
USCRN	USA	5, 10, 20	111	87
OK Mesonet	Oklahoma	5, 25, 60	118	77
OzNet	Australia	4, 45	42	18
All Networks			***406***	***311***

TABLE 3. Overview of sparse networks, with indication of the sensor depths and number of sites (N) used here.

	Reference Pixel		Surface Soil Moisture									Root Zone Soil Moisture								
			ubRMSE [m^3m^{-3}]			Bias [m^3m^{-3}]			R [-]			ubRMSE [m^3m^{-3}]			Bias [m^3m^{-3}]			R [-]		
Site Name	ID	Horiz. Scale [km]	NRv4	*L4_SM Vv2030*	95% Conf. Interval	NRv4	*L4_SM Vv2030*	95% Conf. Interval	NRv4	*L4_SM Vv2030*	95% Conf. Interval	NRv4	*L4_SM Vv2030*	95% Conf. Interval	NRv4	*L4_SM Vv2030*	95% Conf. Interval	NRv4	*L4_SM Vv2030*	95% Conf. Interval
REMEDHUS	**03013602**	**36**	**0.027**	***0.028***	**±0.005**	**0.068**	***0.072***	**±0.007**	**0.78**	***0.77***	**±0.08**	n/a	n/a	n/a	n/a	n/a	n/a	n/a	n/a	n/a
	03010903	9	0.024	*0.029*	±0.005	0.142	*0.150*	±0.007	0.52	*0.46*	±0.14	n/a	n/a	n/a	n/a	n/a	n/a	n/a	n/a	n/a
	03010908	9	0.035	*0.038*	±0.007	0.013	*0.015*	±0.009	0.68	*0.63*	±0.10	n/a	n/a	n/a	n/a	n/a	n/a	n/a	n/a	n/a
Reynolds Creek	**04013603**	**36**	**0.032**	***0.027***	**±0.008**	**0.025**	***0.033***	**±0.011**	**0.65**	***0.78***	**±0.18**	n/a	n/a	n/a	n/a	n/a	n/a	n/a	n/a	n/a
	04010907	9	0.032	*0.031*	±0.010	-0.005	*-0.001*	±0.013	0.33	*0.45*	±0.26	n/a	n/a	n/a	n/a	n/a	n/a	n/a	n/a	n/a
	04010910	9	0.036	*0.029*	±0.018	0.042	*0.039*	±0.022	0.62	*0.76*	±0.22	n/a	n/a	n/a	n/a	n/a	n/a	n/a	n/a	n/a
Yanco	**07013601**	**36**	**0.065**	***0.038***	**±0.019**	**0.005**	***0.036***	**±0.025**	**0.83**	***0.93***	**±0.08**	**0.017**	***0.020***	**±0.010**	**-0.100**	***-0.079***	**±0.012**	**0.89**	***0.95***	**±0.17**
	07010902	9	0.084	*0.057*	±0.017	-0.017	*0.010*	±0.023	0.83	*0.91*	±0.07	n/a	n/a	n/a	n/a	n/a	n/a	n/a	n/a	n/a
	07010916	9	0.068	*0.043*	±0.019	0.028	*0.068*	±0.025	0.77	*0.91*	±0.10	n/a	n/a	n/a	n/a	n/a	n/a	n/a	n/a	n/a
Carman	**09013610**	**36**	**0.025**	***0.038***	**±0.004**	**-0.080**	***-0.066***	**±0.005**	**0.60**	***0.45***	**±0.10**	n/a	n/a	n/a	n/a	n/a	n/a	n/a	n/a	n/a
	09010906	9	0.031	*0.050*	±0.005	0.043	*0.080*	±0.007	0.53	*0.26*	±0.14	n/a	n/a	n/a	n/a	n/a	n/a	n/a	n/a	n/a
Ngari	**12033601**	**36**	**0.046**	***0.037***	**±0.017**	**0.000**	***0.011***	**±0.022**	**0.78**	***0.77***	**±0.22**	n/a	n/a	n/a	n/a	n/a	n/a	n/a	n/a	n/a
Walnut Gulch	**16013603**	**36**	**0.033**	***0.031***	**±0.003**	**0.030**	***0.039***	**±0.005**	**0.58**	***0.67***	**±0.09**	n/a	n/a	n/a	n/a	n/a	n/a	n/a	n/a	n/a
	16010906	9	0.028	*0.030*	±0.003	0.019	*0.034*	±0.005	0.69	*0.68*	±0.08	n/a	n/a	n/a	n/a	n/a	n/a	n/a	n/a	n/a
	16010907	9	0.026	*0.031*	±0.003	0.039	*0.050*	±0.005	0.68	*0.66*	±0.08	n/a	n/a	n/a	n/a	n/a	n/a	n/a	n/a	n/a
	16010913	9	0.036	*0.034*	±0.006	0.075	*0.081*	±0.009	0.60	*0.65*	±0.15	n/a	n/a	n/a	n/a	n/a	n/a	n/a	n/a	n/a
Little Washita	**16023602**	**36**	**0.037**	***0.033***	**±0.004**	**-0.004**	***-0.015***	**±0.006**	**0.73**	***0.81***	**±0.05**	**0.029**	***0.024***	**±0.005**	**-0.037**	***-0.043***	**±0.007**	**0.87**	***0.88***	**±0.09**
	16020907	9	0.037	*0.034*	±0.006	-0.015	*-0.026*	±0.009	0.71	*0.78*	±0.07	0.030	*0.030*	±0.009	-0.039	*-0.043*	±0.012	0.82	*0.76*	±0.16
Fort Cobb	**16033602**	**36**	**0.038**	***0.034***	**±0.004**	**0.027**	***0.028***	**±0.005**	**0.70**	***0.78***	**±0.06**	**0.024**	***0.025***	**±0.004**	**0.020**	***0.025***	**±0.005**	**0.76**	***0.79***	**±0.12**
	16030911	9	0.043	*0.038*	±0.006	0.027	*0.033*	±0.008	0.71	*0.77*	±0.07	0.029	*0.032*	±0.007	0.020	*0.031*	±0.009	0.69	*0.74*	±0.18
	16030916	9	0.039	*0.038*	±0.005	-0.004	*-0.008*	±0.007	0.60	*0.68*	±0.07	0.027	*0.030*	±0.006	-0.029	*-0.026*	±0.009	0.61	*0.62*	±0.22
Little River	**16043602**	**36**	**0.044**	***0.035***	**±0.004**	**0.102**	***0.093***	**±0.006**	**0.68**	***0.76***	**±0.09**	**0.033**	***0.025***	**±0.005**	**0.073**	***0.063***	**±0.007**	**0.81**	***0.84***	**±0.11**
	16040901	9	0.045	*0.038*	±0.005	0.128	*0.115*	±0.007	0.58	*0.64*	±0.13	0.039	*0.032*	±0.006	0.125	*0.109*	±0.008	0.55	*0.65*	±0.20
St Josephs	16060907	9	0.053	*0.050*	±0.012	0.111	*0.094*	±0.017	0.43	*0.60*	±0.25	n/a	n/a	n/a	n/a	n/a	n/a	n/a	n/a	n/a
South Fork	**16073602**	**36**	**0.058**	***0.044***	**±0.008**	**0.077**	***0.045***	**±0.011**	**0.23**	***0.65***	**±0.11**	**0.040**	***0.031***	**±0.006**	**0.024**	***-0.012***	**±0.009**	**0.11**	***0.56***	**±0.26**
	16070909	9	0.064	*0.043*	±0.008	0.029	*-0.009*	±0.011	0.11	*0.71*	±0.12	0.045	*0.029*	±0.007	-0.035	*-0.081*	±0.010	0.06	*0.70*	±0.25
	16070911	9	0.070	*0.053*	±0.010	0.075	*0.039*	±0.013	0.08	*0.62*	±0.12	0.044	*0.031*	±0.008	0.028	*-0.014*	±0.010	0.03	*0.58*	±0.29
Monte Buey	**19023601**	**36**	**0.044**	***0.034***	**±0.010**	**-0.043**	***-0.035***	**±0.014**	**0.65**	***0.79***	**±0.07**	n/a	n/a	n/a	n/a	n/a	n/a	n/a	n/a	n/a
	19020902	9	0.037	*0.029*	±0.009	-0.038	*-0.025*	±0.012	0.60	*0.83*	±0.09	n/a	n/a	n/a	n/a	n/a	n/a	n/a	n/a	n/a
Tonzi Ranch	**25013601**	**36**	**0.042**	***0.032***	**±0.010**	**0.029**	***0.047***	**±0.014**	**0.92**	***0.95***	**±0.06**	n/a	n/a	n/a	n/a	n/a	n/a	n/a	n/a	n/a
	25010911	9	0.046	*0.037*	±0.011	0.033	*0.044*	±0.015	0.90	*0.93*	±0.07	n/a	n/a	n/a	n/a	n/a	n/a	n/a	n/a	n/a
Kenaston	**27013601**	**36**	**0.038**	***0.034***	**±0.005**	**0.010**	***0.012***	**±0.007**	**0.51**	***0.63***	**±0.09**	**0.020**	***0.023***	**±0.005**	**-0.043**	***-0.041***	**±0.007**	**0.53**	***0.63***	**±0.27**
	27010910	9	0.034	*0.035*	±0.009	0.009	*0.016*	±0.012	0.61	*0.61*	±0.12	n/a	n/a	n/a	n/a	n/a	n/a	n/a	n/a	n/a
	27010911	9	0.040	*0.040*	±0.008	-0.020	*-0.021*	±0.011	0.56	*0.54*	±0.11	0.018	*0.023*	±0.003	-0.069	*-0.070*	±0.004	0.63	*0.63*	±0.18
Valencia	41010906	9	0.025	*0.023*	±0.005	0.104	*0.109*	±0.007	0.44	*0.51*	±0.16	n/a	n/a	n/a	n/a	n/a	n/a	n/a	n/a	n/a
Niger	**45013601**	**36**	**0.030**	***0.030***	**±0.005**	**-0.001**	***0.022***	**±0.007**	**0.40**	***0.62***	**±0.20**	n/a	n/a	n/a	n/a	n/a	n/a	n/a	n/a	n/a
	45010902	9	0.032	*0.033*	±0.004	0.006	*0.030*	±0.006	0.31	*0.52*	±0.17	n/a	n/a	n/a	n/a	n/a	n/a	n/a	n/a	n/a
Benin	**45023601**	**36**	**0.050**	***0.048***	**±0.016**	**0.059**	***0.037***	**±0.021**	**0.62**	***0.66***	**±0.20**	n/a	n/a	n/a	n/a	n/a	n/a	n/a	n/a	n/a
	45020902	9	0.050	*0.047*	±0.016	0.053	*0.036*	±0.021	0.68	*0.72*	±0.17	n/a	n/a	n/a	n/a	n/a	n/a	n/a	n/a	n/a
TxSON	**48013601**	**36**	**0.041**	***0.036***	**±0.008**	**0.084**	***0.086***	**±0.010**	**0.82**	***0.87***	**±0.08**	**0.036**	***0.033***	**±0.016**	**0.034**	***0.038***	**±0.020**	**0.92**	***0.86***	**±0.19**
	48010902	9	0.039	*0.037*	±0.005	0.120	*0.121*	±0.007	0.73	*0.80*	±0.08	0.032	*0.029*	±0.008	0.086	*0.092*	±0.010	0.76	*0.79*	±0.18
	48010911	9	0.049	*0.044*	±0.008	0.124	*0.127*	±0.011	0.76	*0.83*	±0.10	0.028	*0.029*	±0.011	0.079	*0.083*	±0.014	0.91	*0.87*	±0.17
HOBE	**67013601**	**36**	**0.030**	***0.035***	**±0.008**	**0.011**	***-0.004***	**±0.010**	**0.78**	***0.71***	**±0.13**	n/a	n/a	n/a	n/a	n/a	n/a	n/a	n/a	n/a
ALL SITES	**AVERAGE**	**36**	**0.040**	***0.035***	**±0.002**	**0.023**	***0.026***	**±0.003**	**0.66**	***0.74***	**±0.03**	**0.028**	***0.026***	**±0.003**	**-0.004**	***-0.007***	**±0.004**	**0.70**	***0.79***	**±0.06**
	AVERAGE	9	0.042	***0.038***	±0.002	0.043	***0.046***	±0.003	0.58	***0.67***	±0.03	0.032	***0.030***	±0.003	0.019	***0.009***	±0.004	0.56	***0.70***	±0.08

TABLE 4. Soil moisture metrics at individual reference pixels and (bottom two rows) averaged over 36-km and 9-km reference pixels. Information for 36-km reference pixels is shown in bold. Italics indicate L4_SM metrics.

	Reference Pixel		Surface Soil Temperature (6am)									Surface Soil Temperature (6pm)								
			ubRMSE [K]			Bias [K]			R [-]			ubRMSE [K]			Bias [K]			R [-]		
Site Name	ID	Horiz. Scale [km]	NRv4	*L4_SM Vv2030*	95% Conf. Interval	NRv4	*L4_SM Vv2030*	95% Conf. Interval	NRv4	*L4_SM Vv2030*	95% Conf. Interval	NRv4	*L4_SM Vv2030*	95% Conf. Interval	NRv4	*L4_SM Vv2030*	95% Conf. Interval	NRv4	*L4_SM Vv2030*	95% Conf. Interval
REMEDHUS	**03013602**	**36**	**2.0**	***1.5***	**±1.1**	**-4.0**	***-3.4***	**±1.3**	**0.98**	***0.99***	**±0.02**	**1.4**	***1.6***	**±1.1**	**-0.7**	***-2.1***	**±1.3**	**0.99**	***0.99***	**±0.02**
	03010903	9	2.2	*1.8*	±1.2	-4.8	*-4.2*	±1.4	0.97	*0.98*	±0.03	1.6	*2.0*	±1.3	-1.8	*-3.3*	±1.5	0.99	*0.99*	±0.02
	03010908	9	1.7	*1.2*	±1.0	-3.8	*-3.1*	±1.1	0.98	*0.99*	±0.02	1.4	*1.4*	±1.2	-0.2	*-1.6*	±1.3	0.99	*0.99*	±0.03
Reynolds Creek	**04013603**	**36**	**1.6**	***1.8***	**±1.9**	**-0.2**	***1.5***	**±1.9**	**0.98**	***0.98***	**±0.05**	**1.8**	***1.6***	**±1.7**	**2.5**	***0.9***	**±1.8**	**0.98**	***0.98***	**±0.04**
	04010907	9	1.4	*1.7*	±1.6	0.3	*2.2*	±1.6	0.98	*0.98*	±0.04	1.7	*1.5*	±1.6	2.4	*0.7*	±1.7	0.98	*0.98*	±0.04
	04010910	9	2.5	*2.5*	±3.2	-2.5	*-1.1*	±3.1	0.96	*0.96*	±0.07	2.3	*2.3*	±2.7	0.1	*-0.9*	±2.7	0.96	*0.96*	±0.07
Yanco	**07013601**	**36**	**1.8**	***1.5***	**±0.7**	**-3.5**	***-2.2***	**±0.8**	**0.97**	***0.98***	**±0.02**	**1.6**	***1.6***	**±0.6**	**0.7**	***-0.5***	**±0.8**	**0.98**	***0.98***	**±0.01**
	07010902	9	1.9	*1.4*	±0.6	-3.1	*-1.8*	±0.8	0.97	*0.98*	±0.02	1.7	*1.6*	±0.5	1.6	*0.3*	±0.7	0.98	*0.98*	±0.02
	07010916	9	2.6	*1.8*	±0.8	-4.2	*-2.9*	±1.0	0.96	*0.98*	±0.03	1.7	*1.6*	±0.5	0.5	*-0.8*	±0.7	0.98	*0.98*	±0.02
Carman	**09013610**	**36**	**2.6**	***2.6***	**±0.9**	**-3.1**	***-2.6***	**±1.2**	**0.93**	***0.93***	**±0.06**	**2.2**	***2.2***	**±0.9**	**1.4**	***0.3***	**±1.1**	**0.95**	***0.95***	**±0.05**
	09010906	9	2.8	*2.7*	±1.0	-3.2	*-2.8*	±1.3	0.93	*0.93*	±0.07	2.3	*2.2*	±0.9	1.2	*0.0*	±1.2	0.95	*0.95*	±0.05
Ngari	**12033601**	**36**	**2.4**	***2.0***	**±1.6**	**-5.2**	***-3.6***	**±1.9**	**0.90**	***0.92***	**±0.27**	**2.8**	***2.4***	**±0.8**	**-9.1**	***-12.5***	**±1.1**	**0.89**	***0.90***	**±0.12**
Walnut Gulch	**16013603**	**36**	**1.4**	***1.2***	**±0.5**	**-1.7**	***-1.5***	**±0.6**	**0.98**	***0.99***	**±0.02**	**1.6**	***1.7***	**±0.5**	**0.2**	***-2.1***	**±0.7**	**0.98**	***0.98***	**±0.02**
	16010906	9	1.7	*1.4*	±0.6	-1.9	*-1.7*	±0.7	0.97	*0.98*	±0.02	1.9	*1.9*	±0.6	1.0	*-1.5*	±0.8	0.98	*0.98*	±0.02
	16010907	9	1.4	*1.3*	±0.6	-3.1	*-2.8*	±0.7	0.98	*0.99*	±0.02	1.7	*1.7*	±0.6	0.2	*-2.2*	±0.8	0.98	*0.98*	±0.02
	16010913	9	2.0	*1.6*	±1.5	-3.0	*-2.6*	±1.7	0.98	*0.99*	±0.06	2.1	*2.3*	±1.1	-0.3	*-2.6*	±1.4	0.98	*0.98*	±0.04
Little Washita	**16023602**	**36**	**1.6**	***1.8***	**±1.0**	**-2.3**	***-1.7***	**±1.2**	**0.98**	***0.98***	**±0.02**	**1.8**	***1.8***	**±1.2**	**0.2**	***-0.5***	**±1.4**	**0.98**	***0.98***	**±0.02**
	16020907	9	1.5	*1.6*	±1.0	-2.1	*-1.5*	±1.2	0.98	*0.98*	±0.02	1.7	*1.7*	±1.1	0.2	*-0.6*	±1.3	0.98	*0.98*	±0.03
Fort Cobb	**16033602**	**36**	**1.5**	***1.5***	**±0.9**	**-2.3**	***-1.8***	**±1.0**	**0.98**	***0.99***	**±0.02**	**1.7**	***1.7***	**±0.9**	**0.3**	***-0.6***	**±1.1**	**0.98**	***0.98***	**±0.02**
	16030911	9	1.3	*1.3*	±0.7	-1.8	*-1.4*	±0.9	0.99	*0.99*	±0.01	1.5	*1.5*	±0.9	0.4	*-0.5*	±1.1	0.99	*0.99*	±0.02
	16030916	9	1.4	*1.5*	±1.4	-1.7	*-1.0*	±1.5	0.97	*0.98*	±0.04	1.4	*1.4*	±1.4	0.8	*0.0*	±1.5	0.98	*0.98*	±0.05
Little River	**16043602**	**36**	**1.5**	***1.5***	**±0.6**	**-3.0**	***-1.8***	**±0.8**	**0.98**	***0.99***	**±0.01**	**1.7**	***1.5***	**±0.7**	**-0.8**	***-1.7***	**±0.9**	**0.98**	***0.98***	**±0.02**
	16040901	9	1.7	*1.6*	±0.6	-2.9	*-1.8*	±0.8	0.98	*0.99*	±0.01	1.8	*1.7*	±0.8	-1.1	*-1.9*	±1.0	0.98	*0.98*	±0.02
St Josephs	16060907	9	1.6	*1.5*	±0.9	-2.0	*-1.3*	±1.1	0.97	*0.98*	±0.02	1.6	*1.5*	±0.8	-0.2	*-0.9*	±1.0	0.98	*0.98*	±0.02
South Fork	**16073602**	**36**	**1.6**	***1.6***	**±1.0**	**-2.3**	***-1.5***	**±1.1**	**0.98**	***0.98***	**±0.02**	**1.7**	***1.7***	**±1.1**	**-0.2**	***-0.9***	**±1.3**	**0.98**	***0.98***	**±0.02**
	16070909	9	1.4	*1.4*	±0.7	-2.0	*-1.2*	±0.9	0.98	*0.98*	±0.02	1.5	*1.5*	±0.8	0.0	*-0.6*	±1.0	0.98	*0.98*	±0.02
	16070911	9	1.6	*1.5*	±0.8	-2.4	*-1.7*	±1.0	0.98	*0.98*	±0.02	1.6	*1.6*	±1.0	-0.3	*-0.9*	±1.2	0.98	*0.98*	±0.02
Monte Buey	**19023601**	**36**	**1.2**	***1.2***	**±0.4**	**-2.6**	***-2.6***	**±0.5**	**0.97**	***0.97***	**±0.02**	**1.6**	***1.7***	**±0.5**	**-0.9**	***-1.9***	**±0.7**	**0.96**	***0.96***	**±0.03**
	19020902	9	n/a	*n/a*	n/a	n/a	*n/a*	n/a	n/a	*n/a*	n/a	1.4	*1.8*	±0.7	0.3	*-1.2*	±0.8	0.97	*0.94*	±0.05
Tonzi Ranch	**25013601**	**36**	n/a	*n/a*	n/a	n/a	*n/a*	n/a	n/a	*n/a*	n/a	n/a	*n/a*	n/a	n/a	*n/a*	n/a	n/a	*n/a*	n/a
	25010911	9	n/a	*n/a*	n/a	n/a	*n/a*	n/a	n/a	*n/a*	n/a	n/a	*n/a*	n/a	n/a	*n/a*	n/a	n/a	*n/a*	n/a
Kenaston	**27013601**	**36**	**1.3**	***1.4***	**±0.9**	**-1.5**	***-1.0***	**±1.0**	**0.98**	***0.97***	**±0.03**	**2.1**	***1.9***	**±1.2**	**1.5**	***0.5***	**±1.4**	**0.95**	***0.96***	**±0.05**
	27010910	9	1.3	*1.0*	±0.6	-1.6	*-1.1*	±0.7	0.98	*0.99*	±0.02	1.8	*1.5*	±0.6	0.7	*-0.3*	±0.8	0.97	*0.98*	±0.03
	27010911	9	1.3	*1.3*	±0.9	-1.7	*-1.2*	±1.0	0.98	*0.97*	±0.03	2.1	*1.8*	±1.0	0.9	*-0.1*	±1.2	0.95	*0.96*	±0.04
Valencia	41010906	9	n/a	*n/a*	n/a	n/a	*n/a*	n/a	n/a	*n/a*	n/a	n/a	*n/a*	n/a	n/a	*n/a*	n/a	n/a	*n/a*	n/a
Niger	**45013601**	**36**	n/a	*n/a*	n/a	n/a	*n/a*	n/a	n/a	*n/a*	n/a	n/a	*n/a*	n/a	n/a	*n/a*	n/a	n/a	*n/a*	n/a
	45010902	9	n/a	*n/a*	n/a	n/a	*n/a*	n/a	n/a	*n/a*	n/a	n/a	*n/a*	n/a	n/a	*n/a*	n/a	n/a	*n/a*	n/a
Benin	**45023601**	**36**	n/a	*n/a*	n/a	n/a	*n/a*	n/a	n/a	*n/a*	n/a	n/a	*n/a*	n/a	n/a	*n/a*	n/a	n/a	*n/a*	n/a
	45020902	9	n/a	*n/a*	n/a	n/a	*n/a*	n/a	n/a	*n/a*	n/a	n/a	*n/a*	n/a	n/a	*n/a*	n/a	n/a	*n/a*	n/a
TxSON	**48013601**	**36**	**1.1**	***1.1***	**±0.3**	**-2.0**	***-1.4***	**±0.4**	**0.99**	***0.99***	**±0.01**	**1.6**	***1.5***	**±0.6**	**-0.8**	***-1.8***	**±0.7**	**0.98**	***0.98***	**±0.02**
	48010902	9	1.3	*1.2*	±0.4	-2.7	*-2.2*	±0.5	0.98	*0.99*	±0.01	1.8	*1.7*	±0.7	-1.6	*-2.6*	±0.9	0.98	*0.98*	±0.02
	48010911	9	1.3	*1.2*	±0.4	-2.3	*-1.8*	±0.5	0.98	*0.99*	±0.01	2.1	*2.1*	±0.8	-1.9	*-2.9*	±1.0	0.98	*0.98*	±0.02
HOBE	**67013601**	**36**	**1.0**	***1.2***	**±0.5**	**-1.1**	***-0.4***	**±0.7**	**0.98**	***0.98***	**±0.02**	**1.1**	***1.2***	**±0.6**	**-0.8**	***-1.5***	**±0.8**	**0.98**	***0.98***	**±0.03**
ALL SITES	**AVERAGE**	**36**	**1.6**	***1.6***	**±0.2**	**-2.5**	***-1.7***	**±0.3**	**0.97**	***0.97***	**±0.01**	**1.8**	***1.7***	**±0.2**	**-0.5**	***-1.7***	**±0.3**	**0.97**	***0.97***	**±0.01**
	AVERAGE	9	1.7	*1.6*	±0.3	-2.5	*-1.8*	±0.3	0.98	*0.98*	±0.01	1.8	*1.7*	±0.3	0.1	*-1.1*	±0.3	0.98	*0.98*	±0.01

1144

1145 TABLE 5. As in Table 4 but for soil temperature metrics.

Sparse Network Subset	Surface Soil Moisture										Root Zone Soil Moisture									
		ubRMSE [m^3m^{-3}]			Bias [m^3m^{-3}]			R [-]				ubRMSE [m^3m^{-3}]			Bias [m^3m^{-3}]			R [-]		
	Number of sites	NRv4	*L4_SM Vv2030*	95% Conf. Interval	NRv4	*L4_SM Vv2030*	95% Conf. Interval	NRv4	*L4_SM Vv2030*	95% Conf. Interval	Number of sites	NRv4	*L4_SM Vv2030*	95% Conf. Interval	NRv4	*L4_SM Vv2030*	95% Conf. Interval	NRv4	*L4_SM Vv2030*	95% Conf. Interval
Forests (IGBP 1-5)	41	0.056	*0.054*	±0.005	0.104	*0.103*	±0.004	0.64	*0.65*	±0.03	34	0.047	*0.045*	±0.005	0.055	*0.055*	±0.005	0.62	*0.64*	±0.08
Open shrublands (IGBP 7)	27	0.037	*0.034*	±0.003	0.016	*0.030*	±0.003	0.66	*0.71*	±0.03	20	0.028	*0.026*	±0.005	-0.008	*0.006*	±0.004	0.66	*0.63*	±0.09
Woody savannas (IGBP 8)	28	0.065	*0.059*	±0.008	0.069	*0.060*	±0.006	0.65	*0.70*	±0.05	23	0.054	*0.048*	±0.010	0.037	*0.025*	±0.013	0.68	*0.70*	±0.13
Grasslands (IGBP 10)	177	0.053	*0.051*	±0.003	0.026	*0.031*	±0.003	0.65	*0.69*	±0.02	130	0.041	*0.042*	±0.006	-0.014	*-0.007*	±0.007	0.72	*0.69*	±0.07
Croplands (IGBP 12)	83	0.060	*0.057*	±0.003	0.026	*0.022*	±0.004	0.60	*0.64*	±0.03	60	0.046	*0.046*	±0.005	0.007	*0.004*	±0.005	0.65	*0.65*	±0.07
Urban/built-up (IGBP 13)	4	0.080	*0.071*	±0.017	0.027	*0.006*	±0.015	0.49	*0.62*	±0.11	3	0.047	*0.049*	±0.020	0.046	*0.032*	±0.019	0.64	*0.63*	±0.32
Crop/natural (IGBP 14)	39	0.060	*0.057*	±0.003	0.033	*0.027*	±0.003	0.66	*0.70*	±0.02	36	0.048	*0.045*	±0.003	0.008	*0.002*	±0.004	0.66	*0.69*	±0.06
Barren/sparse (IGBP 16)	2	0.033	*0.026*	±0.005	0.004	*0.016*	±0.004	0.61	*0.70*	±0.08	1	0.016	*0.017*	±0.020	-0.028	*-0.031*	±0.014	0.95	*0.92*	±0.35
Inside mask	279	0.056	*0.054*	±0.002	0.030	*0.028*	±0.002	0.64	*0.67*	±0.02	206	0.045	*0.044*	±0.003	-0.001	*-0.003*	±0.003	0.66	*0.66*	±0.04
Outside mask	127	0.052	*0.049*	±0.003	0.074	*0.078*	±0.002	0.64	*0.67*	±0.02	105	0.041	*0.040*	±0.004	0.040	*0.042*	±0.004	0.65	*0.65*	±0.05
Average (all sites)	**406**	**0.054**	***0.052***	**±0.002**	**0.050**	***0.051***	**±0.002**	**0.64**	***0.67***	**±0.01**	**311**	**0.044**	***0.042***	**±0.002**	**0.016**	***0.016***	**±0.003**	**0.66**	***0.66***	**±0.03**

TABLE 6. Sparse network metrics by land cover (IGBP class) and by the mask of the L4_SM core validation site accuracy requirement (section 3c). Italics indicate L4_SM metrics. Averages are based on a clustering algorithm (section 3c).

Figure Captions

Fig. 1. Schematic of the L4_SM algorithm and data product. See section 2 for details and abbreviations.

Fig. 2. (a) Surface soil moisture from (black solid line) L4_SM Vv2030, (light blue solid line) NRv4, and (red dots) *in situ* measurements at the 36-km Little Washita reference pixel #16023602. (b) As in (a) but for root-zone soil moisture. See Table 4 for performance metrics.

Fig. 3. As in Figure 2 but for the 36-km Little River reference pixel #16043602.

Fig. 4. As in Figure 2 but for the 9-km South Fork reference pixel #16070911.

Fig. 5. (a) ubRMSE ($m^3\ m^{-3}$), (b) bias ($m^3\ m^{-3}$), and (c) R (dimensionless) for L4_SM Vv2030 and NRv4 surface and root-zone soil moisture vs. core validation site measurements, averaged across all 9-km and 36-km reference pixels. Error bars indicate 95% confidence intervals. The thick horizontal line in panel (a) represents the L4_SM accuracy requirement of ubRMSE ≤ 0.04 $m^3\ m^{-3}$.

Fig. 6. As in Figure 5 but for surface soil temperature at 6am and 6pm, with ubRMSE and bias in K.

Fig. 7. ubRMSE ($m^3\ m^{-3}$) vs. sparse network measurements for L4_SM Vv2030 (a,b) surface and (c,d) root-zone soil moisture. (a,c) United States sites include (circles) SCAN, (inverted triangles) USCRN, and (squares) OK Mesonet. (b,d) Australian sites are from OzNet. Gray shading indicates areas with low or modest vegetation cover and topographic complexity that are within the mask of the SMAP accuracy requirement (section 3c).

Fig. 8. As in Figure 7 but for the time series correlation coefficient R (dimensionless).

Fig. 9. (a,b) ubRMSE ($m^3\ m^{-3}$), (c,d) bias ($m^3\ m^{-3}$), and (e,f) R (dimensionless) for L4_SM Vv2030 and NRv4 surface and root-zone soil moisture vs. sparse network measurements, averaged across sites (a,c,e) within the mask and (b,d,f) outside the mask shown by the gray shading in Figures 7 and 8. Averages are based on a clustering algorithm (section 3c). Error bars indicate 95% confidence intervals.

1191

1192 **Figures**

1193

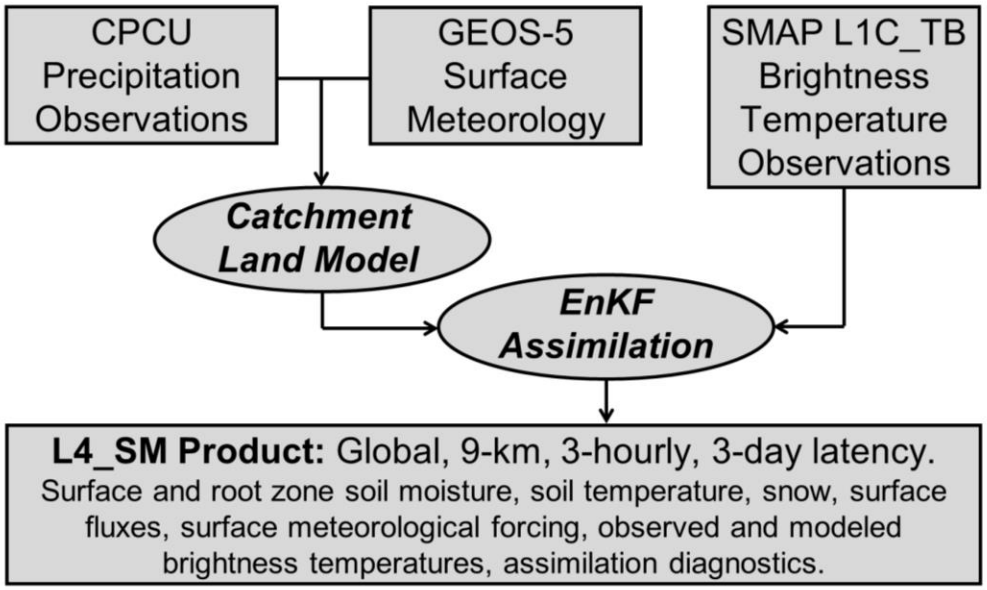

1194

1195 Fig. 1. Schematic of the L4_SM algorithm and data product. See section 2 for details and

1196 abbreviations.

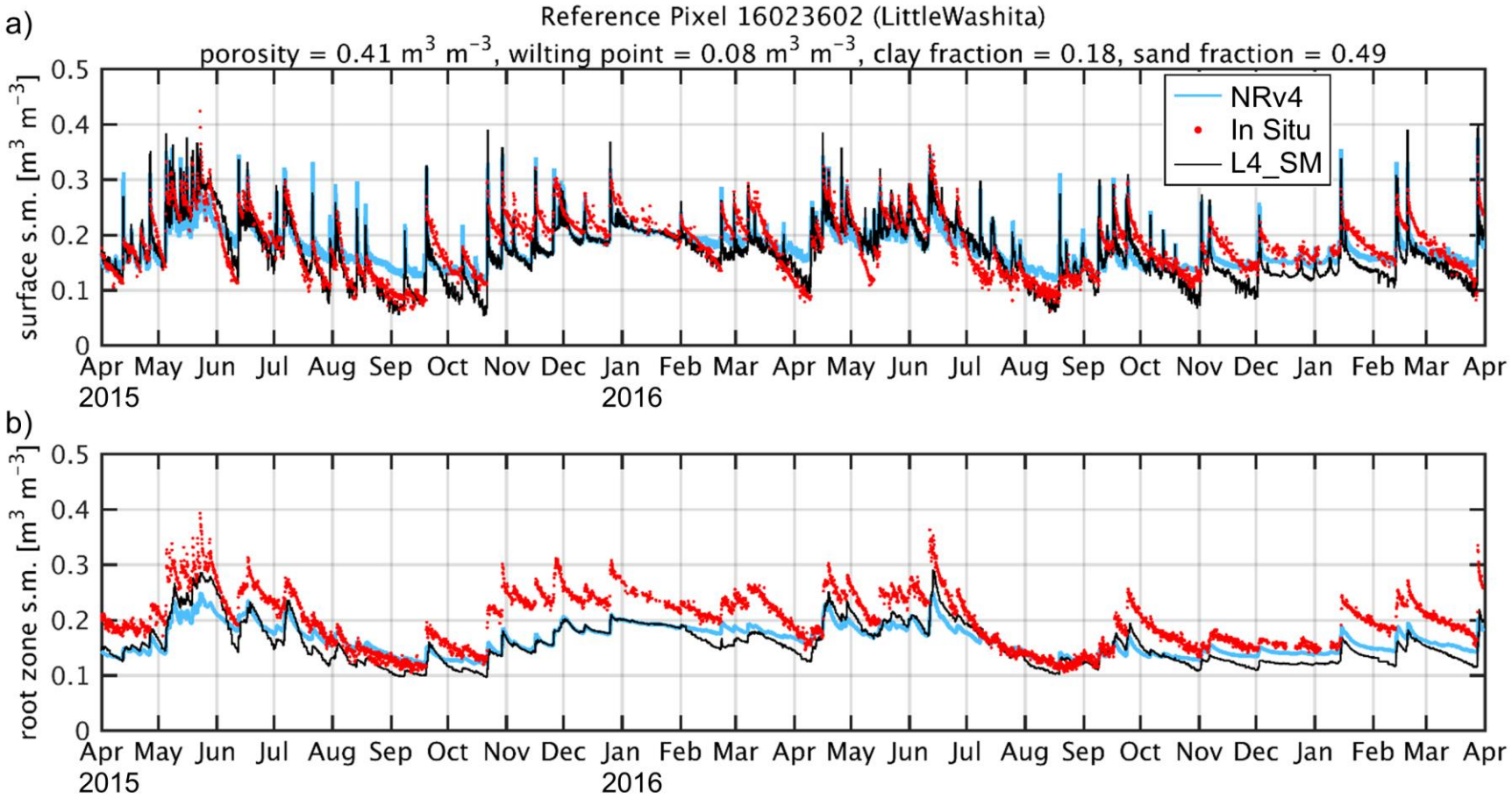

Fig. 2. (a) Surface soil moisture from (black solid line) L4_SM Vv2030, (light blue solid line) NRv4, and (red dots) *in situ* measurements at the 36-km Little Washita reference pixel #16023602. (b) As in (a) but for root-zone soil moisture. See Table 4 for performance metrics.

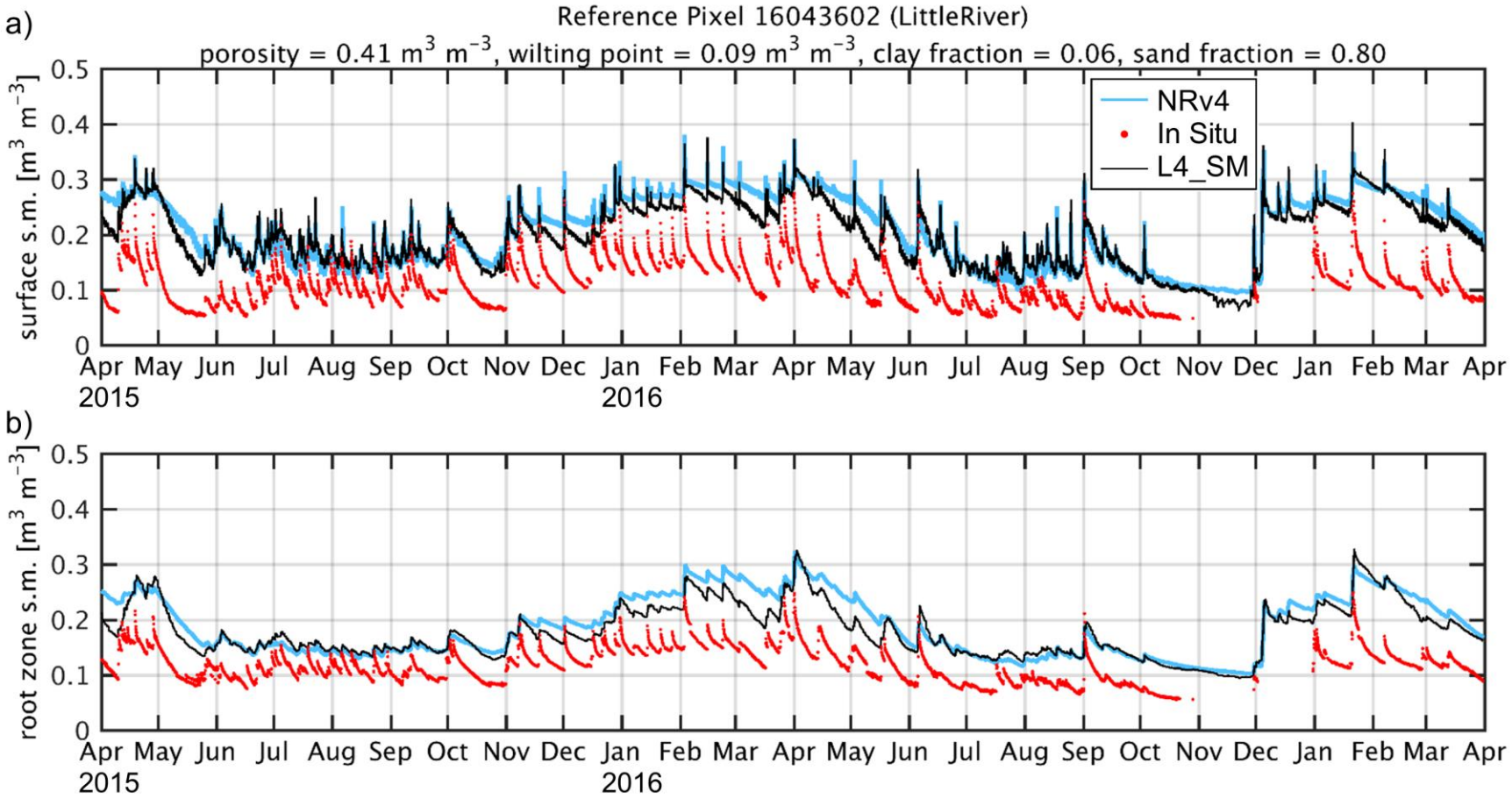

1201

1202 Fig. 3. As in Figure 2 but for the 36-km Little River reference pixel #16043602.

1203

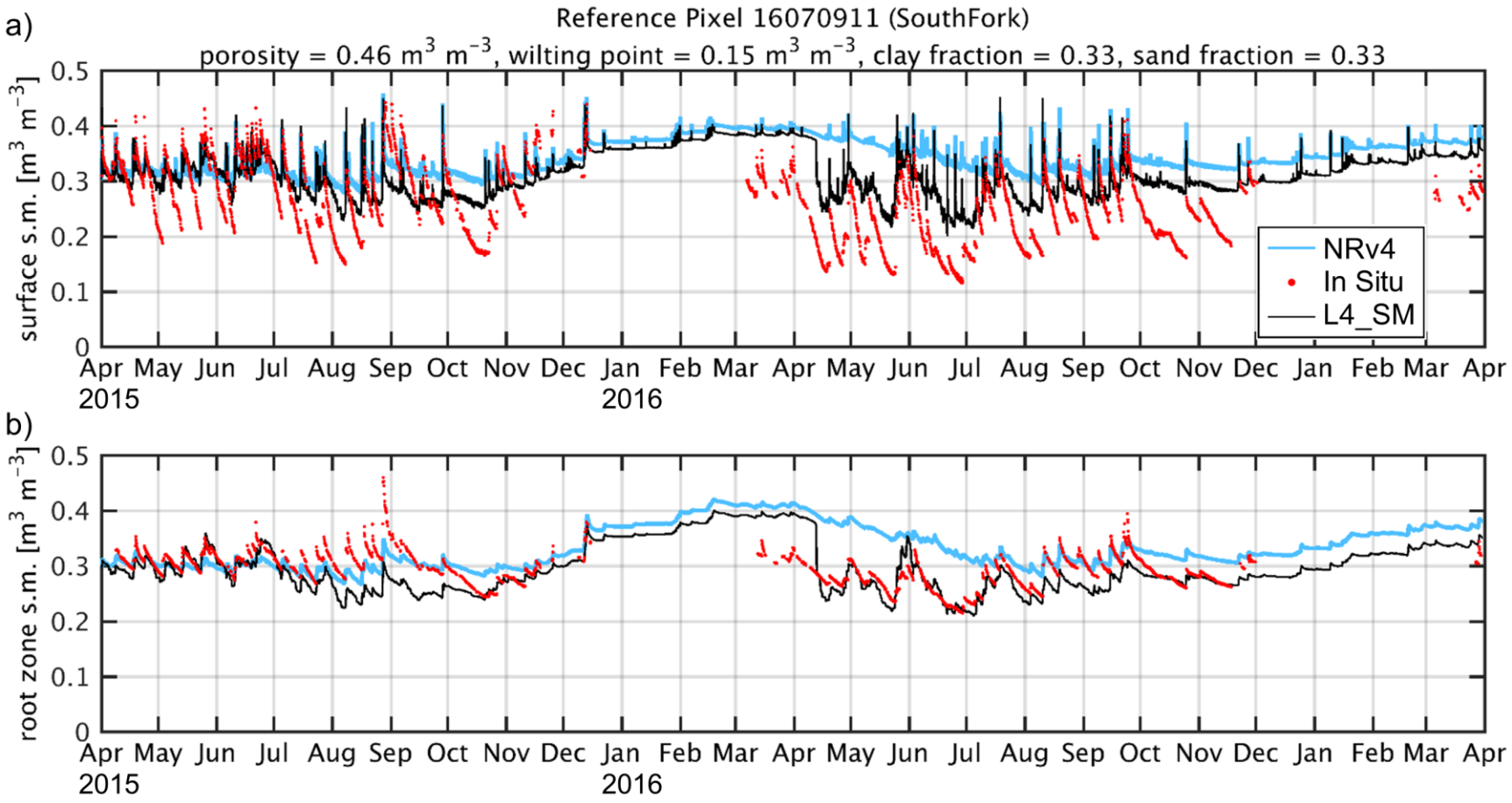

1204

1205 Fig. 4. As in Figure 2 but for the 9-km South Fork reference pixel #16070911.

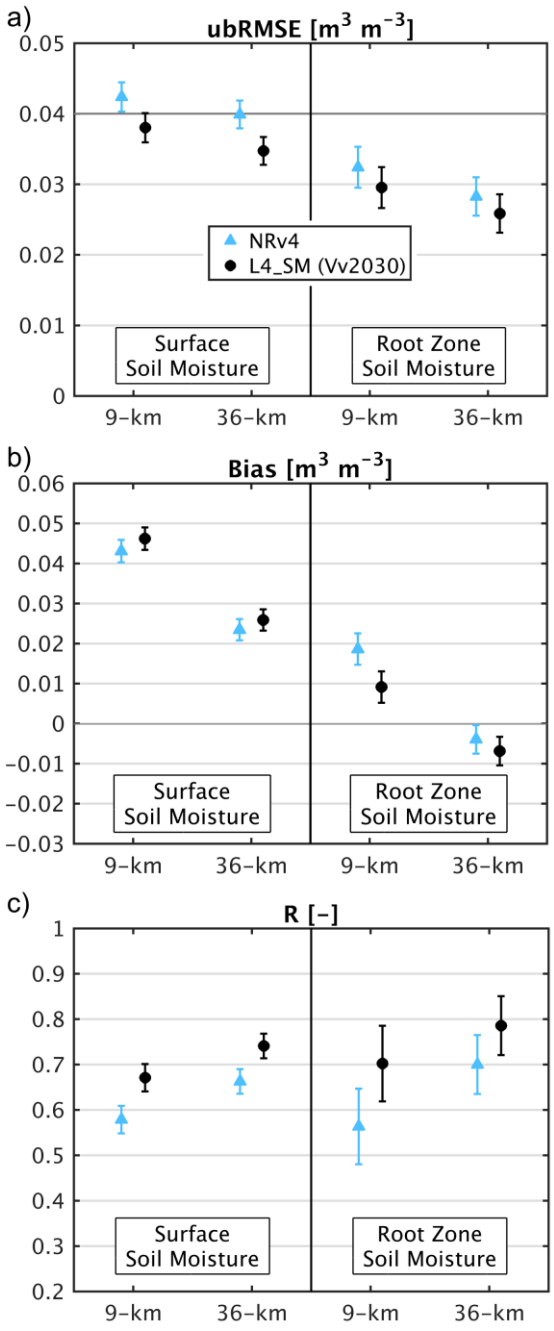

1206

1207 Fig. 5. (a) ubRMSE (m^3 m^{-3}), (b) bias (m^3 m^{-3}), and (c) R (dimensionless) for L4_SM Vv2030
1208 and NRv4 surface and root-zone soil moisture vs. core validation site measurements, averaged
1209 across all 9-km and 36-km reference pixels. Error bars indicate 95% confidence intervals. The
1210 thick horizontal line in panel (a) represents the L4_SM accuracy requirement of ubRMSE $\leq$ 0.04
1211 m^3 m^{-3}.

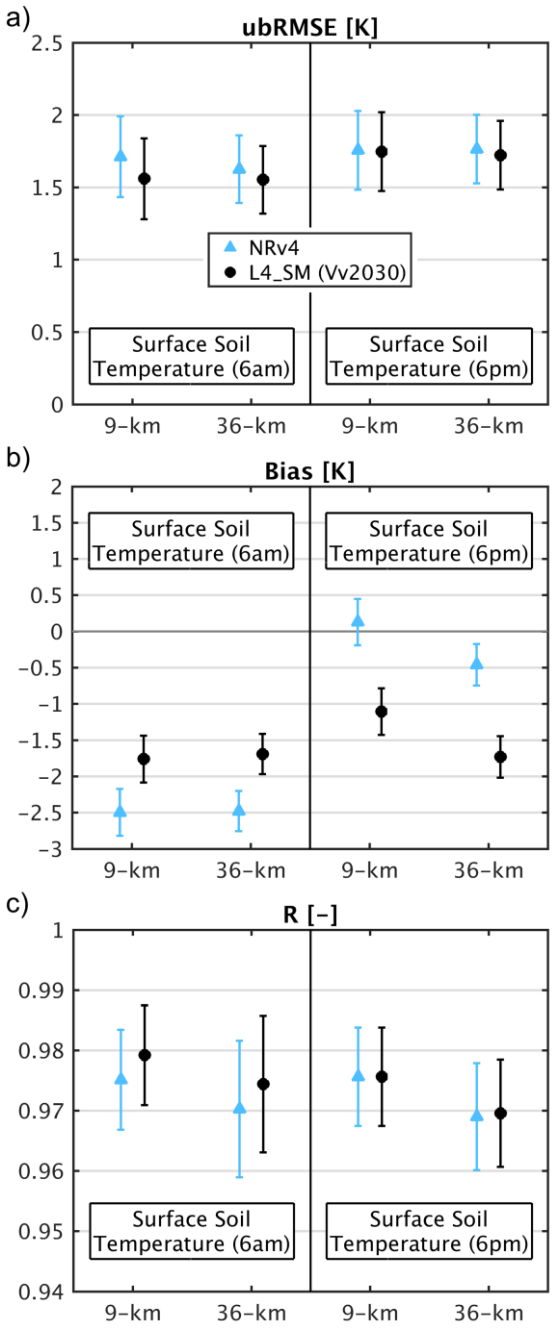

1212

1213 Fig. 6. As in Figure 5 but for surface soil temperature at 6am and 6pm, with ubRMSE and bias

1214 in K.

1215

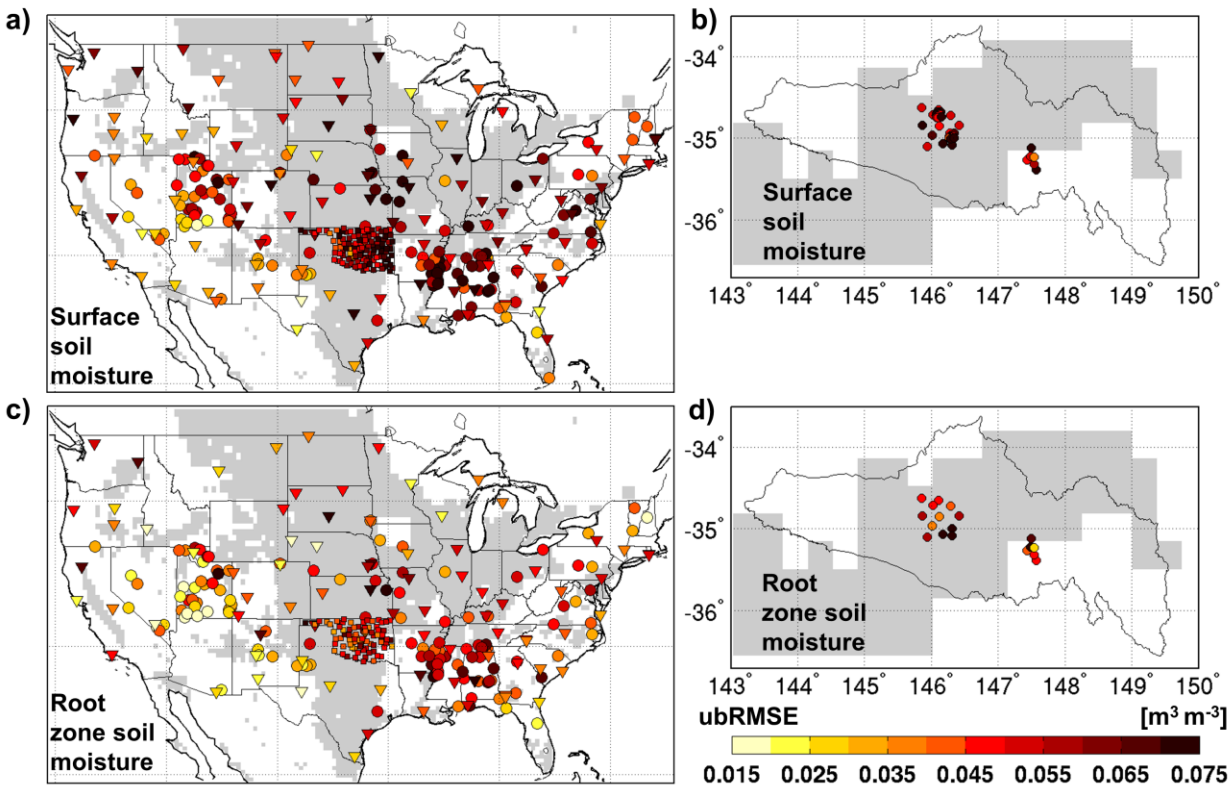

1216

1217 Fig. 7. ubRMSE (m^3 m^{-3}) vs. sparse network measurements for L4_SM Vv2030 (a,b) surface

1218 and (c,d) root-zone soil moisture. (a,c) United States sites include (circles) SCAN, (inverted

1219 triangles) USCRN, and (squares) OK Mesonet. (b,d) Australian sites are from OzNet. Gray

1220 shading indicates areas with low or modest vegetation cover and topographic complexity that are

1221 within the mask of the SMAP accuracy requirement (section 3c).

1222

1223

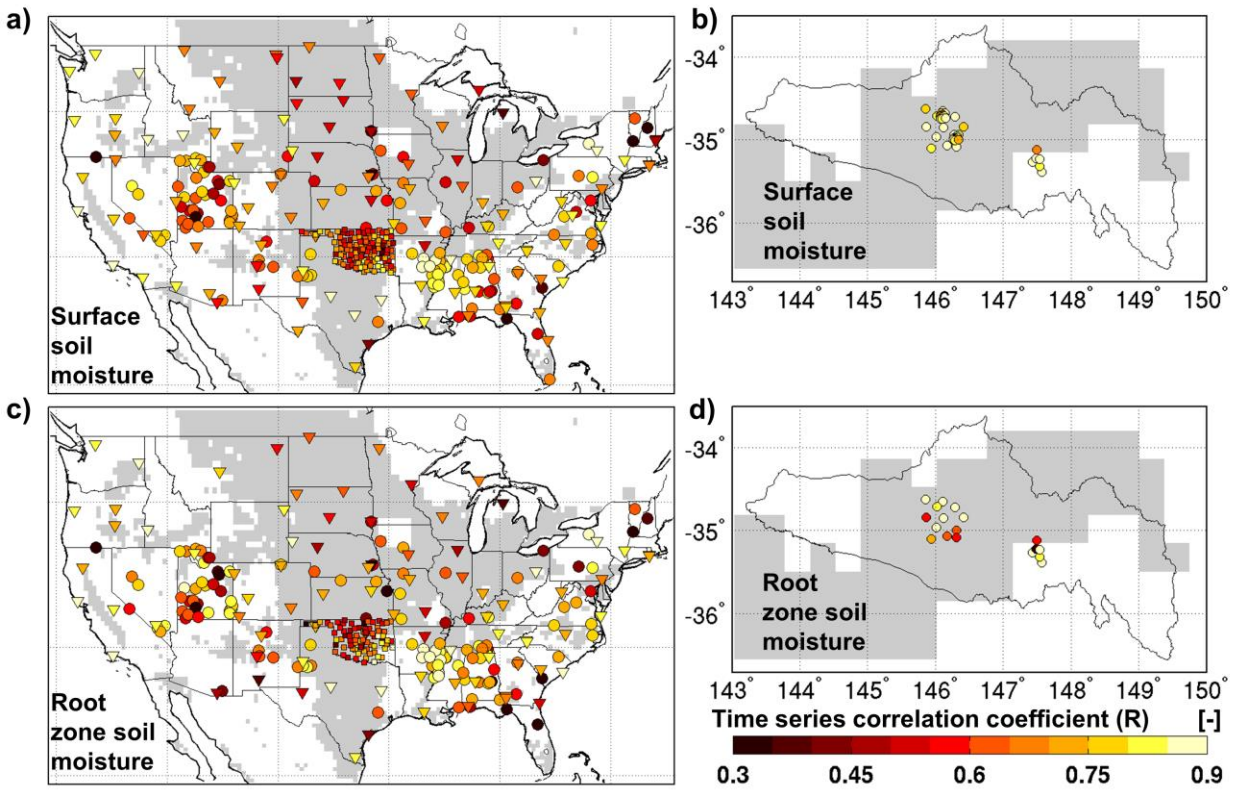

1224

1225 Fig. 8. As in Figure 7 but for the time series correlation coefficient R (dimensionless).

1226

1227

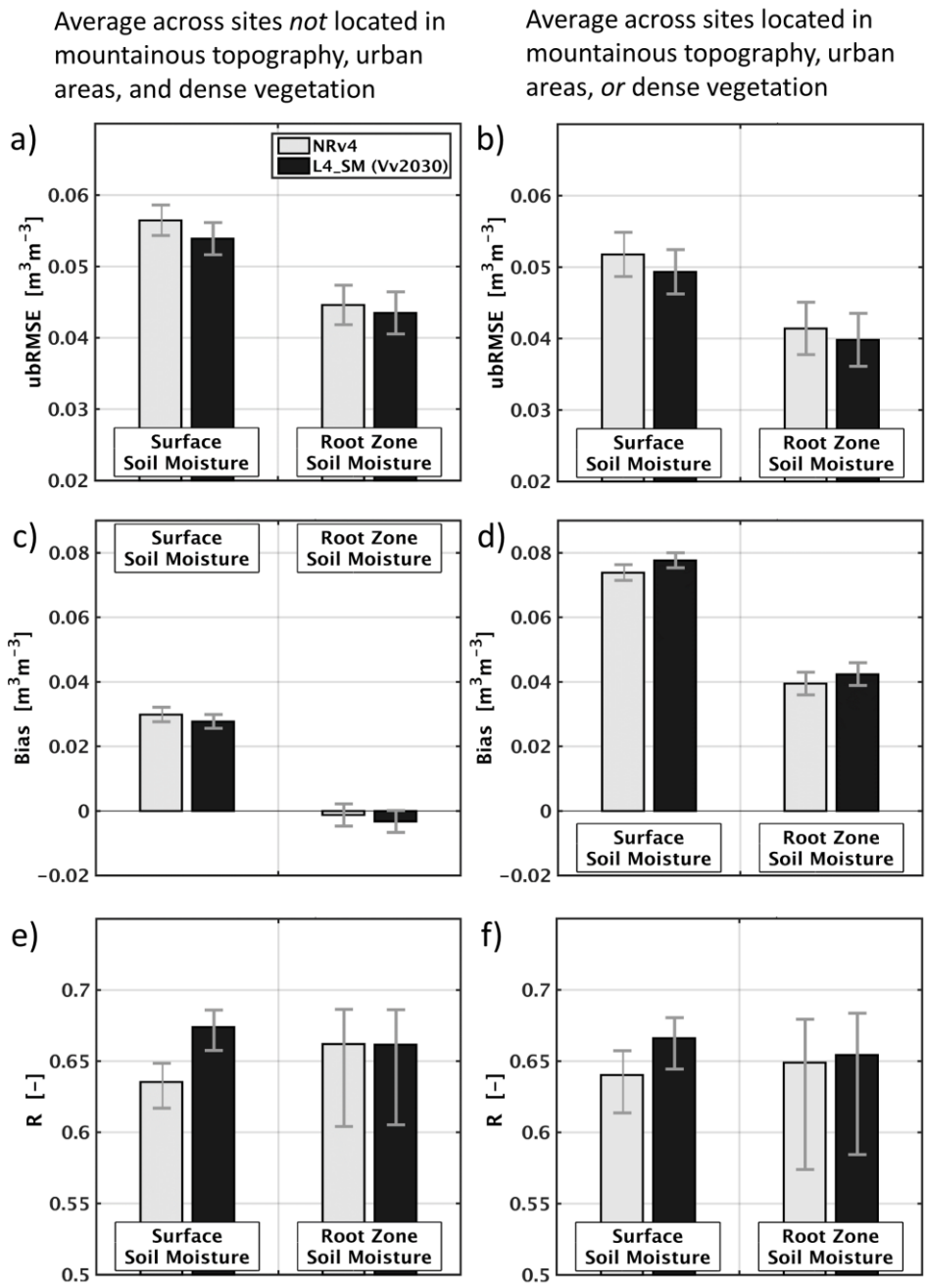

Fig. 9. (a,b) ubRMSE (m^3 m^{-3}), (c,d) bias (m^3 m^{-3}), and (e,f) R (dimensionless) for L4_SM Vv2030 and NRv4 surface and root-zone soil moisture vs. sparse network measurements, averaged across sites (a,c,e) within the mask and (b,d,f) outside the mask shown by the gray shading in Figures 7 and 8. Averages are based on a clustering algorithm (section 3c). Error bars indicate 95% confidence intervals.